Global Climate Impacts of Greenland and Antarctic Glacial Melt: A Comparative Study

Qian Li[a], John Marshall[a], Craig D. Rye[a,b], Anastasia Romanou[b], David Rind[b], and Maxwell Kelley[b]

[a] *Department of Earth, Atmospheric, and Planetary Sciences, Massachusetts Institute of Technology, Cambridge, MA, USA*

[b] *NASA Goddard Institute for Space Studies, New York, NY, USA*

Corresponding author: Qian Li, qian_li@mit.edu

ABSTRACT: Continental glaciers have been melting at an accelerating rate over recent decades in both Greenland and Antarctica. Fresh water release around Greenland might be expected to initiate a climate response which is distinct, and perhaps different from, that associated with Antarctic melt-water release. Which might elicit the greatest response, and what mechanisms are involved? In this study, we apply "Climate Response Functions" (CRFs) to guide a series of meltwater perturbation experiments using a fully coupled climate system model to explore. In the atmosphere, meltwater forcing from both glaciers drive cooling of air temperatures, circulation strengthening and sea ice expansion. In the ocean, upper and lower meridional overturning cells both experience a slowdown. The Atlantic meridional overturning circulation (AMOC) shows a pronounced decline in response to Greenland melt with subsurface cooling. In response to Antarctic glacial melt, instead, Antarctic Bottom Water slows down and the subsurface ocean warms. For small melt-water rates — up to 2000 Gt yr^{-1} or so — the response to both forcings is rather linear. However, as the forcing increases to 5000 Gt yr^{-1} or so, the response becomes non-linear. Because of a collapse of the AMOC at high melt-rates, the climate response exceeds that which would be expected for linear change. In contrast, the response to Antarctic melt is sub-linear at high forcing amplitudes because the northward expansion of sea-ice is halted by warm surface waters. Finally, we use CRFs and linear convolution theory to make projections of key climate variables given freshwater melt scenarios.

1. Introduction

The cryospheres of Greenland and Antarctica represent the largest land store of freshwater over the globe which, should they melt and flow in to the ocean, could contribute 7.5 m and 58 m to global sea level respectively (Morlighem et al. 2017; Fretwell et al. 2013). Recent observations have shown that these glaciers are melting at an accelerating rate (Paolo et al. 2015; Rignot et al. 2019; Mouginot et al. 2019; Shepherd et al. 2018, 2020). Between 1992–2011 and 2012–2017, the rate of net land ice loss has risen from 119 Gt yr^{-1} to 244 Gt yr^{-1} in Greenland (Shepherd et al. 2020) and from 76 Gt yr^{-1} to 219 Gt yr^{-1} in Antarctica (Shepherd et al. 2018). Since the 1990s, their combined contribution to mean sea level has been 18 mm or so, of which perhaps 10 mm came from Greenland due to increased surface melting and ice dynamical imbalance (Shepherd et al. 2020) and 8 mm or so due to basal melting and iceberg calving around Antarctica (Shepherd et al. 2018). In future climate scenarios assuming high (RCP8.5) greenhouse gas emissions, by the year 2100 the net melt rate of Greenland and Antarctic glaciers is projected to exceed 500 Gt yr^{-1} and 5000 Gt yr^{-1}, respectively (Golledge et al. 2019). Such melt rates would lead to a sea-level rise in excess of 25 cm or so (Golledge et al. 2019; DeConto and Pollard 2016).

Polar glacial melt contributes not only to sea level but also initiates climate change through its effect, for example, on the ocean's sea-ice extent and vertical overturning circulation. One might expect the impacts of Greenland glacial melt to be different from that of Antarctic glacial melt because they act in different hemispheres and perturb different parts of the climate system. For example, it is thought that Antarctic meltwater spreading to the proximal ocean initiates surface cooling and freshening trends across the Southern Ocean (Bronselaer et al. 2018; Rye et al. 2020). Enhanced basal melting of ice shelves particularly around Antarctica (Rignot et al. 2013; Depoorter et al. 2013; Adusumilli et al. 2020), has been identified as an important cause of sea ice expansion by intensifying the oceanic stratification and suppressing deep convection and its associated vertical heat exchange (Hellmer 2004; Bintanja et al. 2013), with impacts on sinking along the margins of Antarctic continent and Antarctic Bottom Water (AABW) (Silvano et al. 2018). Accelerated glacial melt around Greenland, meanwhile, can reduce deep ocean ventilation via a slowdown in the formation rate of North Atlantic Deep Water (NADW) originating in the Nordic (Greenland-Iceland-Norwegian) seas (Böning et al. 2016), and a weakening of the Atlantic meridional overturning circulation (AMOC) (Caesar et al. 2018). Glacial melt in one hemisphere can also affect the other due to its influence on the atmosphere above and the ocean below. For example increased southern stratification around Antarctica due to glacial melt could ultimately lead to a strengthening of the ocean's AMOC (Weaver et al. 2003) yet which is being damped by Greenland melt. Such competing climate impacts become even more intriguing when it is realised that increasing differences between the melt rates of Greenland and Antarctic glaciers are expected in the coming decades (Golledge et al. 2019; Slater et al. 2020) with the Antarctic source likely to increasingly dominate over Greenland as time proceeds.

Addressing these issues is important not least because experiments undertaken for the latest Coupled Model Intercomparison Project Phase 6 (CMIP6) (Eyring et al. 2016) do not account for glacial melt in future climate projections. That said, many recent climate model simulations have applied meltwater scenarios either around Greenland (Hu et al. 2011; Weijer et al. 2012; Putrasahan et al. 2019; Marson et al. 2021) or Antarctica (Bakker and Prange 2018; Bronselaer et al. 2018; Lago and England 2019; Moorman et al. 2020; Rye et al. 2020; Mackie et al. 2020). Taken together, these studies suggest that over the next two centuries Greenland melt is projected to significantly weaken the AMOC and lessen surface warming mainly in the Arctic and the subpolar North Atlantic Regions (Hu et al. 2011). By 2100, Antarctic melt is projected to drive a series of notable changes, including a reduction in global surface air temperature, an increase in sea ice formation, subsurface ocean warming around Antarctica associated with a marked diminution of Antarctic Bottom Water and a northward shift of the ITCZ (Bronselaer et al. 2018).

The primary motivation of the current study is to (i) identify the key mechanisms which control the response of the climate system to Greenland and Antarctic melt and (ii) to quantify the efficacy of Greenland vs Antarctic melt in instigating global climate change. We will quantitatively contrast the global impacts of Greenland and Antarctic glacial melt through a response function analysis of a fully coupled climate model. We undertake three sets of experiments in which the same amount of perturbed meltwater is released along the land-ocean boundary of Greenland and Antarctica, both separately and together. We carry out the experiments in the framework provided by "Climate Response Functions" (CRFs) (Hasselmann et al. 1993; Marshall et al. 2014, 2017a), which enable us to compare the relative contributions of different hemispheric sources on the global climate.

Our paper is organized as follows. In Section 2, the coupled model and experimental design are described. Sections 3 and 4 respectively contrast the global responses and mechanisms of

Greenland and Antarctic melt. Section 5 discusses the response functions for glacial melt and use them to make future projections of climatically important parameters, such as surface air temperature, strength of the AMOC and ice extent. Finally, Section 6 contains a discussion and concluding remarks.

2. The coupled model and experimental design

a. The global climate model

We employ the E2.1-G version of the NASA Goddard Institute for Space Studies (GISS) Earth system model, denoted GISS-E2.1-G (Kelley et al. 2020; Miller et al. 2021; Nazarenko et al. 2022). GISS-E2.1-G is a coupled climate model designed to simulate the earth system comprising representations of the atmosphere, ocean, land and cryosphere. The atmospheric model component has a horizontal resolution of 2°× 2.5°latitude by longitude and 40 vertical pressure layers. The vertical coordinate transitions from a terrain-following sigma tropospheric representation below 150 hPa to constant-pressure stratospheric layers above this level, all the way up to the model top at 0.1 hPa. In this E2.1-G version, a new option facilitates a smooth transition centered at 100 hPa with a half-width of approximately 30 hPa. The dynamical core, atmospheric mixing, convection and boundary layer models are described in more detail in (Kelley et al. 2020).

The ocean model component of E2.1-G version has a horizontal resolution of 1°× 1.25°latitude by longitude and 40 mass layers in the vertical. It is mass-conserving with a free surface and natural surface boundary conditions for heat and freshwater fluxes (Russell et al. 1995). The model employs a version of the boundary layer K-profile parameterization (KPP) of vertical mixing (Large et al. 1994) and the Gent and McWilliams (GM) parameterization (Gent et al. 1995) with variable coefficients (Visbeck et al. 1997) for eddy tracer fluxes induced by mesoscale baroclinic turbulence. In E2.1-G, the parameterization of mesoscale eddy transport is updated with a moderate-complexity 3-D mesoscale diffusivity inspired by the studies presented in Marshall et al. (2017b). The vertical diapycnal diffusivity incorporates a new tidal mixing scheme that improves the representation of the AMOC. Additional developments include the use of higher-order advection schemes (Prather 1986), finer upper-ocean layering and more realistic representation of flow through straits that affect property distributions in marginal seas (Kelley et al. 2020).

The sea-ice model component consists of two mass layers within each of which are two thermal layers. Sea ice salinity and tracer values are calculated on the atmospheric grid in the horizontal and the mass layers in the vertical. Sea-ice dynamics is based on a formulation of the standard viscous-plastic rheology (Zhang and Rothrock 2000). Sea-ice thermodynamics includes a "Brine Pocket" (BP) parameterization (Bitz and Lipscomb 1999) that allows salt to play a more active role in the specific heat and melt rates of the sea ice. The ice-sheet component is coupled to the ocean model via an idealized representation of melting ice-bergs, using an ice-berg array function. This is designed such that the meltwater input mimics observations of ice berg calving (Tournadre et al. 2016). Based on the mass and energy associated with net snow accumulation over the ice sheets, iceberg calving fluxes into the adjacent oceans are be adjusted over a 10 year relaxation time enabling the model to reach a long-term mass equilibrium under changed climate forcings (Schmidt et al. 2014).

As documented in (Kelley et al. 2020; Rye et al. 2020), our model has a pleasingly realistic climatology in a long pre-industrial control simulation, particularly in its representation of the southern hemisphere atmosphere, ocean and sea-ice distributions.

b. Experimental design

As summarised in Table 1, we consider three meltwater scenarios in which melt water is released along the land-ocean boundary of Greenland or Antarctica separately or together. In each case, a step-function forcing is applied in which the melt rate is instantaneously stepped up from zero to 500 Gt yr^{-1} in one experiment, 2000 Gt yr^{-1} in another and finally 5000 Gt yr^{-1} to yield three experiments for each scenario (Fig. 1), or nine in all. These amplitudes are inspired by current and projected meltwater rates, as noted above. The perturbed meltwater fluxes and associated cooling anomalies, stemming from extraction of the latent heat required to melt ice, are uniformly distributed in the upper 200 meters following the mask shown in Fig. 2.

In order to contrast the global impacts and mechanisms, all nine idealized perturbation experiments are initiated from a long pre-industrial control and then run on in parallel for 50 years. The experiments in which a small perturbation of 500 Gt yr^{-1} is carried out employ 10 ensemble members enabling us to dampen the effect of internal variability through averaging. The ones which assume much larger perturbations of 2000 Gt yr^{-1} and 5000 Gt yr^{-1} have a more robust response and so need employ only one ensemble member. For the CRFs and linear convolution analyses, all the simulations are extended out to 150 years. This enables us to explore longer timescales and particularly temporal variability of the AMOC. The control experiments carried out alongside these perturbations do not employ any anomalous forcing. The difference between concurrent periods of perturbation and control are analyzed to minimize the influence of model drift on our results.

Note that in our figures the range of the colormap scales linearly with the magnitude of the three meltwater forcing schemes, enabling us to examine the linearity of atmospheric and ocean responses to meltwater forcing.

c. Freshwater pathways

As a broad check on the behavior of our solutions, we present the temporal evolution and spatial distribution of sea surface salinity (SSS) anomalies obtained in response to our three forcings. As shown in the three time series in Fig. 1, the anomalous SSS adjustment reaches a new quasi-steady state in about 10 years. Due to the different land-ocean distributions, the surface freshening is confined to a limited geographic area around Greenland but extends over a larger area across the Southern Ocean around Antarctica. In the Greenland scenario, surface freshening spreads primarily along the Labrador Current in the 500 Gt yr^{-1} and 2000 Gt yr^{-1} cases (Figs. 2a and 2c), but has a wider spatial impact across the subpolar North Atlantic in the 5000 Gt yr^{-1} case (Fig. 2e). As a result, SSS decreases by -0.05 psu and -0.26 psu around Greenland (45°–80°N, 5°–65°W) respectively with a forcing of 500 Gt yr^{-1} and 2000 Gt yr^{-1}, close to a linear scaling. However, when the forcing reaches 5000 Gt yr^{-1}, SSS changes intensify dramatically with a decrease of -1.39 psu. In the Antarctic scenario, the anomalous SSS scales roughly linearly with magnitude in all three forcing schemes, with a decrease of -0.02 psu, -0.11 psu and -0.21 psu in the Antarctic sectors (50°–90°S, 0°–360°E), respectively (Figs. 2b, 2d and 2f). The linearity of the response, or otherwise, will be discussed in more detail as our account proceeds.

In the ocean interior, the freshwater pathways are different in the Greenland and Antarctic scenarios. In response to Greenland melt, anomalous freshening penetrates into the abyssal ocean at high-northern latitudes (Figs. 3a, 3c and 3e). In response to Antarctic melt, in the midlatitudes of the Southern Ocean, anomalous freshening mostly extends down to 1 km depth, following the pathways of formation and subduction of mode and intermediate waters. At high-southern latitudes, the surface freshens but the deep ocean becomes saltier (Figs. 3b, 3d and 3f).

3. Differing Global impacts of Greenland and Antarctic melt

a. Global surface response

To contrast the large-scale impacts from Greenland and Antarctic melt, surface air temperature anomalies are presented from our Greenland only, Antarctic only and combined perturbation experiments in Fig. 4. The surface air temperature experiences a substantial cooling particularly local to the source of meltwater input. In the Greenland scenario, with a relatively small forcing of 500 Gt yr^{-1} and 2000 Gt yr^{-1}, the anomalous surface cooling is apparent in the subpolar North Atlantic (Figs. 4a and 4b). In contrast, the surface cooling occurs largely across the Northern Hemisphere in the 5000 Gt yr^{-1} case (Fig. 4c). Specifically, the global-mean surface air temperature decreases -0.01°C, -0.09°C and -0.68°C in response to, respectively, the 50-year meltwater forcing of 500 Gt yr^{-1}, 2000 Gt yr^{-1} and 5000 Gt yr^{-1} (Figs. 4a-c). In the 5000 Gt yr^{-1} forcing case the response is greater than would be expected if the response was linear. By comparison, in the Antarctic scenario, anomalous surface cooling covers a much wider area across the southern hemisphere. As the forcing amplitude increases, the global-mean surface air temperature decreases by -0.06°C, -0.25°C and -0.46°C, respectively (Figs. 4d-f). In the 5000 Gt yr^{-1} case (Fig. 4f) the response is less than would be expected if the response was linear. A comparison among all nine cases shows that the anomalous surface air temperature scales linearly with forcing magnitude moving from 500 Gt yr^{-1} to 2000 Gt yr^{-1} but, as mentioned, this linear relationship breaks down in the 5000 Gt yr^{-1} case. Furthermore, the anomalous surface air temperature in the simultaneous Greenland and Antarctic scenario is close to the sum of Greenland and Antarctica separately (Figs. 4g-i). The global-scale cooling is dominated by Antarctic melt in the 500 Gt yr^{-1} and 2000 Gt yr^{-1} cases, but is surpassed by Greenland melt when the forcing reaches 5000 Gt yr^{-1}.

b. Atmospheric and ocean response

The zonal-mean atmospheric and ocean temperature anomalies are further examined from all the nine perturbation experiments (Fig. 5). In the atmosphere, glacial melt drives an anomalous cooling over the full vertical extent of the troposphere. With the 50-year meltwater forcing of 500 Gt yr^{-1}

and 2000 Gt yr^{-1}, the anomalous southern hemisphere cooling due to Antarctic melt (Figs. 5d and 5e) is stronger and extends more equatorward to the tropics than the northern hemisphere cooling due to Greenland melt (Figs. 5a and 5b). When the Greenland meltwater forcing is increased to 5000 Gt yr^{-1}, the northern hemisphere cooling becomes dramatically intensified. Instead, when the Antarctic meltwater forcing is increased to 5000 Gt yr^{-1}, the southern hemisphere cooling becomes less than linear. The interior ocean temperature has opposite responses to meltwater forcing in the two hemispheres: an anomalous ocean cooling north of 45°N due to Greenland melt and an anomalous ocean warming south of 45°S due to Antarctic melt. With an increase in forcing from 500 Gt yr^{-1} to 5000 Gt yr^{-1} around Greenland, the anomalous ocean cooling amplifies substantially (Figs. 5a-c). In contrast, anomalous ocean warming responds in a sub-linear way to glacial melt around Antarctica (Figs. 5d-f).

Glacial melt also drives large-scale changes in atmospheric and ocean meridional overturning circulations (MOCs), shown in Fig. 6. Here we quantify the atmospheric MOC in sverdrups (Sv), where 1 Sv=10^9 kg s^{-1} (Czaja and Marshall 2006). This definition is used because it enables us to use the same unit for both the atmosphere and ocean overturning streamfunctions. The climatological mean atmospheric MOC contains three hemispherically symmetric cells: the Hadley cell, Ferrel cell and Polar cell. In both the Greenland and Antarctic scenarios, the 50-year mean anomalous MOC shows a strengthening in Ferrel cell and an equatorward extent of Hadley cell. These changes in atmospheric circulations are more evident with larger meltwater forcing (Figs. 6c and 6f). By comparison, the climatological mean ocean MOC includes two global-scale thermohaline overturning cells: an upper cell linked to the AMOC and a lower cell driven by AABW formation and export (Marshall and Speer 2012). With the enhanced stratification due to meltwater injection, the upper and lower cells both experience a significant slowdown. As the forcing increase from 500 Gt yr^{-1} to 5000 Gt yr^{-1}, the upper cell greatly declines (Figs. 6a-c), but the lower cell is weakened less than a linear decrease (Figs. 6d-f).

4. Contrast of mechanisms controlling the climate response to Greenland and Antarctic glacial melt

a. Sea ice response

The global impacts of Greenland and Antarctic melt are reflections of common but also distinct mechanisms at work in each hemisphere. In both scenarios enhanced upper-ocean stratification due to meltwater anomalies suppresses convection and upward ocean heat transport, resulting in the anomalous surface cooling and sea ice growth (Zhang 2007; Bintanja et al. 2013; Pauling et al. 2016). Anomalous sea ice growth is further intensified due to enhanced surface cooling through reflection of more incoming solar radiation back out to space in the positive ice–albedo feedback. Indeed, the increase in sea ice coverage is evident in both Greenland and Antarctic scenarios (Fig. 7). In the Antarctic scenario, sea ice expands over a greater geographic area in longitude (Figs. 7b, 7d and 7f), causing and coinciding with hemispheric surface cooling anomalies observed around Antarctica (Figs. 4d-f). In a recent study, Rye et al. (2022) highlighted that the widely distributed sea ice can cause a reduction in water vapor from the high southern-latitudes to the tropics, which can further drive a global-scale cooling via a negative water vapor feedback. This could compensate greenhouse-gas-driven global warming by potentially 10 to 30% by the mid-century. In the Greenland scenario, due to a very different land-ocean distribution, sea ice covers only a limited area. Specifically, the sea ice expands mainly along the Labrador Sea in the 500 Gt yr^{-1} and 2000 Gt yr^{-1} cases (Figs. 7a and 7c), and also across the Irminger Sea and past over the Denmark Strait in the 5000 Gt yr^{-1} case (Fig. 7e). Because this sea ice coverage is more geographically confined than that of hemispheric surface cooling (Figs. 4a-c), it is likely that other mechanisms are at work in inducing northern hemisphere surface cooling in the Greenland scenario.

Furthermore, the temporal evolution of sea ice coverage reveals two different types of non-linear response in the two scenarios. In the Greenland case, the sea ice edge, referred to as the latitude of 15 percent sea ice concentration, expands as the forcing magnitude increases from 500 Gt yr^{-1} to 2000 Gt yr^{-1} (Figs. 8a and 8b), but expands dramatically from 67°N to 53°N when the forcing is 5000 Gt yr^{-1} (Figs. 8c and 8d). This sudden jump suggests a *greater-than-linear* response of sea ice growth in the Northern Hemisphere. In the Antarctic scenario, the sea ice coverage increases gradually (Fig. 8h), but the sea ice edge cannot expand too far north due to the presence of warm surface waters: it is found at 61°S, 59°S and 58.8°S in the 500 Gt yr^{-1}, 2000 Gt yr^{-1} and 5000 Gt yr^{-1} experiments, respectively (Figs. 8e-g). This limitation of sea ice edge expansion indicates the other type of *less-than-linear* response of sea ice growth in the Southern Hemisphere.

b. AMOC response

Another important mechanism is the influence of glacial melt on the strength of the AMOC, which largely controls the magnitude of cross-equatorial heat transport and hence the asymmetric temperature response (Delworth et al. 1993; Stouffer et al. 2007; Marshall et al. 2014; Buckley and Marshall 2016). Here we define AMOC strength as the maximum of the Atlantic overturning streamfunction at 45°N. Greenland melt contributes to a pronounced AMOC decline (Fig. 9a-c), which is in agreement with a recent observation-based inference (Rahmstorf et al. 2015) and many other modeling studies (Caesar et al. 2018; Thornalley et al. 2018; Boers 2021). The degree of AMOC decline is also sensitive to the magnitude of meltwater forcing and the response is not linear. As Greenland meltwater forcing increases to 5000 Gt yr^{-1}, the AMOC strength during 50 years decreases by a remarkable ~50% (-11.09 Sv) (Fig. 9c). Meanwhile AMOC strength is relatively insensitive to Antarctic melt rates, increasing by only 0.32 Sv in Antarctic-only forcing runs even at very large forcing (Fig. 9f)[1]. When both Greenland and Antarctic melt are operative, the AMOC response is dominated by Greenland and shows a decline much as found when only Greenland is operative (Figs. 9g-i)

We further investigate the temporal evolution of AMOC strength in Fig. 10. To examine the long-term impact of AMOC decline, six simulations with the two large forcing perturbations of 2000 Gt yr^{-1} and 5000 Gt yr^{-1} in three meltwater scenarios are extended out to 150 years. The AMOC overall transits to another steady state with some fluctuations but with reduced amplitude in about 50 years from all six simulations. In the Greenland scenario, the AMOC strength weakens by ~19.5% (-4.38 Sv) during 150 years with the forcing of 2000 Gt yr^{-1}, which turns out to be not sufficient for a critical transition point to collapse (Fig. 10a). Instead, the AMOC eventually collapses when the forcing reaches 5000 Gt yr^{-1} (Fig. 10a). By contrast, when forcing is from Antarctica, the AMOC exhibits anomalously more frequent fluctuations with the two forcing schemes of 2000 Gt yr^{-1} and 5000 Gt yr^{-1}, and these fluctuations dampen down over time (Fig. 10b). Again, the evolution of

[1](Weaver et al. 2003) argue that a change in the potential density relationship between the inflow of fresh Antarctic Intermediate Water (AAIW) and NADW can lead to enhanced formation of NADW and thence the AMOC.

AMOC strength is dominated by Greenland melt because the influence of Antarctic melt is small by comparison (Fig. 10c).

5. Response functions for glacial melt

a. Climate response functions

Figure 11 shows modeled time series and fitted CRF curves of anomalies in surface air temperature, sea ice extent, AMOC strength anomalies and AABW transport, all scaled per unit forcing. Here we define AABW transport as the minimum of the global overturning streamfunction between 40°S and 50°S, which also reflects the changes in lower cell. Plotted in this way, curves fall on top of one-another if the response changes linearly as the magnitude of meltwater forcing changes from 500 Gt yr^{-1}, 2000 Gt yr^{-1} to 5000 Gt yr^{-1}. Analytical CRF curves are superimposed, constructed to fit the ensemble means. Following Marshall et al. (2014), the fitted curves are calculated as the sum of two exponential functions corresponding to a 'fast' and 'slow' response, expressed as:

$$CRF \times F_{step} = T_f \left(1 - e^{-t/\tau_f}\right) + T_s \left(1 - e^{-t/\tau_s}\right), \tag{1}$$

where F_{step} in Gt yr^{-1} is the scaling factor representing the magnitude of the step function in meltwater forcing, T_f and τ_f are the coefficients of fast and slow responses, T_s and τ_s for the slow response, and t is the time in years.

From Figure 11, we see that the CRFs of surface air temperature and sea ice extent anomalies have a similar form in their respective hemispheres. Furthermore, the CRFs of surface cooling and sea ice growth reveal a linear response as the forcing magnitude increases from 500 Gt yr^{-1} to 2000 Gt yr^{-1} in the Northern Hemisphere due to Greenland melt (Figs. 11a and 11g) and in the Southern Hemisphere due to Antarctic melt (Figs. 11e and 11k). At these forcing levels, the response to Antarctic melt is greater relative to Greenland. But at a forcing of 5000 Gt yr^{-1}, however, we observe massive surface cooling and sea ice growth leading to a greater-than-linear response in the Northern Hemisphere (Figs. 11a and 11g). This is a consequence of a dramatic decline and indeed collapse of the AMOC (Figs. 10a and 11m), as discussed in Orihuela-Pinto et al. (2022). In contrast, in the case of an Antarctic melt of 5000 Gt yr^{-1}, the CRF response is less-than-linear (Figs. 11e and 11k). This weaker response is likely due to the fact that the sea ice edge cannot push further north of ~59°S (Fig. 8g) because SSTs out in in the open ocean are too warm to sustain ice. The CRF of AABW transport anomalies also shows a similar less-than-linear response to Antarctic melt (Fig. 11q). That said, Antarctic melt leads to a very significant reduction in AABW, analogous to the collapse of AMOC in response to Greenland melt. Finally, by comparing CRFs in the simultaneous Greenland and Antarctic scenarios, we see that glacial melt in Greenland and Antarctica plays the dominant role in their respective hemispheres (Fig. 11). The CRFs of these variables have no significant and persistent response in the other hemisphere, and are thus set to zero in the fitted curves (Figs. 11b, 11d, 11h, 11j, 11n and 11p).

b. Projections based on linear convolution theory

By applying linear convolution theory, as set out in (Hasselmann et al. 1993; Marshall et al. 2014, 2017a), we can make projections of climate variables of interest given a postulated time series of meltwater forcing perturbation, thus:

$$\mathcal{P}(t) = \int_0^t CRF|_{\mathcal{P}}\,(t-t')\,\frac{\partial F}{\partial t}\,(t')\,dt', \tag{2}$$

where F (in Gt yr^{-1}) is the prescribed meltwater forcing perturbation time-series, $CRF|_{\mathcal{P}}$ (scaled per unit forcing) is the transient response of a climate variable to the step-change in meltwater forcing, $\mathcal{P}$ is the response to the forcing timeseries and t is the time.

To make a projection, we must assume a forcing function $F(t)$ and its time derivative — required in Eq. (2) — for both Greenland and Antarctica. It appears that the ice mass loss rates of both Greenland and Antarctic glaciers have been accelerating over recent decades (Shepherd et al. 2018, 2020): we estimate them using a linear regression based on satellite observations of ice sheets since 2002 (Watkins et al. 2015). We find that the loss rate during the historical period 2002–2021 ($F|_{2002}$) to be 271.4 Gt yr^{-1} for Greenland and 144.7 Gt yr^{-1} for Antarctica (Fig. 12). Based on future climate projections under the RCP8.5 scenario, we assume the loss rate in 2100 ($F|_{2100}$) to be 568 Gt yr^{-1} for Greenland and 5047 Gt yr^{-1} for Antarctica, following the estimates given in Golledge et al. (2019). Using the loss rates in 2002 ($F|_{2002}$) and 2100 ($F|_{2100}$), we obtain a gross estimate of the linear increase in the forcing, $\partial F/\partial t$, over the period 2002–2100 of 3 Gt yr^{-2} for Greenland and 50 Gt yr^{-2} for Antarctica (Fig. 12). These are then used to carry out the integral in Eq. (2) after multiplying by the appropriate CRF. Note that the melt rate over the 21st century from Antarctica ranges from 500 Gt yr^{-1}, 2000 Gt yr^{-1} and 5000 Gt yr^{-1}, reaching a level that is almost one order of magnitude greater than the rate from Greenland of 500 Gt yr^{-1}.

Figure 13 presents projections of the response of key climate variables to forcing from Greenland and Antarctic, and their sum, so that we can better contrast their relative contributions. We use the CRF in the Greenland scenario appropriate to 500 Gt yr^{-1} and that for Antarctica the 2000 Gt yr^{-1} curve. Consistent with our detailed calculations using the full model, Antarctica dominates in the Southern Hemisphere, inducing surface cooling, sea ice expansion and weakening of AABW transport (Figs. 13b, 13d and 13f). In the Northern Hemisphere, Greenland forcing dominates, but surface cooling and sea ice expansion are roughly one to two orders of magnitude smaller than that in the Southern Hemisphere (Figs. 13a and 13c). In addition, our projections suggests that melt over Greenland will lead to a reduction in AMOC strength of only 0.45 Sv or so by the end of century (Fig. 13e). In contrast, Antarctic forcing will lead to a 10.2 Sv reduction in AABW transport by the end of the century. Recent studies suggest that the AABW decline may be critical to recent and future abyssal ocean warming (Purkey and Johnson 2010; Li et al. 2022), with century-long implications for ocean carbon uptake, ocean deoxygenation, and the global cycling of nutrients. Such a marked reduction in AABW production induced by Antarctic glacial melt could play a key role.

6. Conclusions and summary

Recent observations show that Antarctic and Greenland glacial ice has been melting at an accelerating rate over recent decades and is projected to continue to melt in the coming century. The addition of anomalous glacial meltwater to the polar oceans is shown to drive multiple significant large-scale climate impacts. These impacts express hemispheric asymmetries due to geographical differences that drive distinct feedback processes and response mechanisms. In this study, using a fully coupled climate system model, we have conducted step-function meltwater perturbation experiments, ranging from 500 Gt yr^{-1} through 2000 Gt yr^{-1} to 5000 Gt yr^{-1} for Greenland and Antarctica, separately and together. This has enabled us to explore and contrast the global impacts of Greenland and Antarctic melt on the climate system.

A broad summary of the changes induced by these glacial discahrges is shown in Fig. 14. In the atmosphere, glacial melt causes significant changes in temperature and circulation, including cooling from the surface to the tropopause, an intensification of the Ferrel cell and poleward expansion of Hadley cell in both hemispheres (top panel in Fig. 14). By comparison, these changes driven by Antarctic melt are greater and across a wider latitudinal extent when the melt rates are in the range 500 Gt/yr and 2000 Gt/yr. In the ocean, the upper and lower cells weaken due to both Greenland and Antarctic melt, respectively, associated with water mass changes in AAIW, NADW and AABW. Meanwhile, we find anomalous cooling in the high northern latitudes due to Greenland melt and anomalous warming around Antarctica due to Antarctic melt (bottom panel in Fig. 14b). It should be noted that subsurface warming around Antarctica could further increase basal melting of ice shelves via a positive feedback (Bronselaer et al. 2018), which has not been addressed in the present study.

The mechanisms controlling the response to Greenland and Antarctic melt are distinct. Overall, glacial melt induces a significant increase in sea ice coverage. As sea ice expands, it leads to anomalous surface cooling via the suppression of upward ocean heat transport and a positive ice-albedo feedback. Antarctic melt can further drive a global-scale cooling due to a reduction in water vapor from the high southern-latitudes to the tropics (Rye et al. 2022). For small forcings, the response is rather linear. However, because the northward extent of sea ice edge is constrained to ~59°S, the response to the strongest of our Antarctic forcings — 5000 Gt yr^{-1} — is sub-linear. In response to Greenland melt, in contrast, anomalous sea ice growth and surface cooling in the north is more geographically confined than in the south. This is because 1) the sea ice growth is limited to a smaller geographic area in longitude and 2) the surface cooling is also modulated by changes in AMOC, which reduces the poleward heat transport to high latitudes in the Atlantic, with a warming at low latitudes that might counteract any reduced water vapor-induced tropical cooling at least at low atmospheric levels. In the Greenland scenario, the AMOC declines gradually as the forcing increases from 500 Gt yr^{-1} to 2000 Gt yr^{-1}, and eventually collapses when the forcing reaches 5000 Gt yr^{-1}. The collapse of AMOC causes dramatic atmospheric and ocean changes: the response is amplifying and also non-linear in the Northern Hemisphere.

In summary and in broad brush, we find that the climate response per unit forcing is linear for small melt rates but, as the forcing increases in magnitude, is less than linear in response to Antarctic forcing but greater than linear in the case of Greenland. This difference is due to the differing mechanisms at work in each case. In the case of Antarctic glacial melt forcing, the response is ultimately sub-linear because the continued expansion of sea-ice outward is capped by the presence of warm waters to the north. In the case of Greenland the response is greater there at large forcing because glacial melt ultimately leads to the collapse of the AMOC. For smaller forcing levels the response to Greenland dominates but for large forcing glacial melt over Antarctica becomes the major player.

We further contrast the relative contributions of Greenland and Antarctic melt through analyses of CRFs, and convolutions based on future melt-rate scenarios. Antarctic melt-rates are projected to be at least one order of magnitude larger than that of Greenland melt by 2100, although Greenland dominates over Antarctica in the historical period. Our results suggest that Antarctic melt will largely affect changes across the Southern Hemisphere, including anomalous surface cooling, sea ice expansion and AABW transport weakening. By comparison, during the 21st century, Greenland melt dominates the response across the Northern Hemisphere, but with at much smaller magnitude.

While our model simulates distinct freshwater pathways due to Greenland and Antarctic melt, the $\sim 1^\circ$ horizontal resolution of ocean model limits to resolve the mesoscale eddies and small-scale topographic features, which influence the western boundary currents (Swingedouw et al. 2022) and shelf circulation (Thompson et al. 2018). In our model, most of the deep water formation is produced from the Labrador and Irminger Seas, but not much from the Greenland, Iceland and Norwegian (GIN) Seas (Pickart and Spall 2007; Lozier et al. 2019). Lerner et al. (2021) suggested that our model has excessive transport of heat into the North Atlantic deep ocean, resulting from relatively deep mixed layer therein. Additionally, our model shows a relatively fast decline of AMOC among the CMIP6 models in response to global warming (Bellomo et al. 2021). In the context of this study, we detect some slight inter-hemispheric climate linkages driven by Antarctic melt, such as the abyssal warming extending across the equator after 50 years and ocean cooling in the north after 100 years (not shown). However, we do not find a clear response of AMOC to Antarctic melt, which may be due to the limited duration of our experiments extending out to only 150 years. The future glacial melt rate is estimated based on the RCP8.5 scenario (Golledge et al. 2019), which represents an upper bound for what is possible, and therefore the “non-linearity” would come into effect early and, according to our analysis, the projected changes would be relatively large. Despite the above caveats, our results robustly contrast the role of Greenland vs Antarctic melt in instigating global climate change.

TABLE 1. Experimental design for meltwater perturbation experiments.

Meltwater (MW) forcing schemes		500 Gt/yr	2000 Gt/yr	5000 Gt/yr
Scenarios	Greenland MW	10 ensembles	1 ensemble	1 ensemble
	Antarctic MW	10 ensembles	1 ensemble	1 ensemble
	Greenland & Antarctic MW	10 ensembles	1 ensemble	1 ensemble
Period		50+100 years	50+100 years	50+100 years
Distribution		Uniformly distributed around the coastline in the upper 200 m		

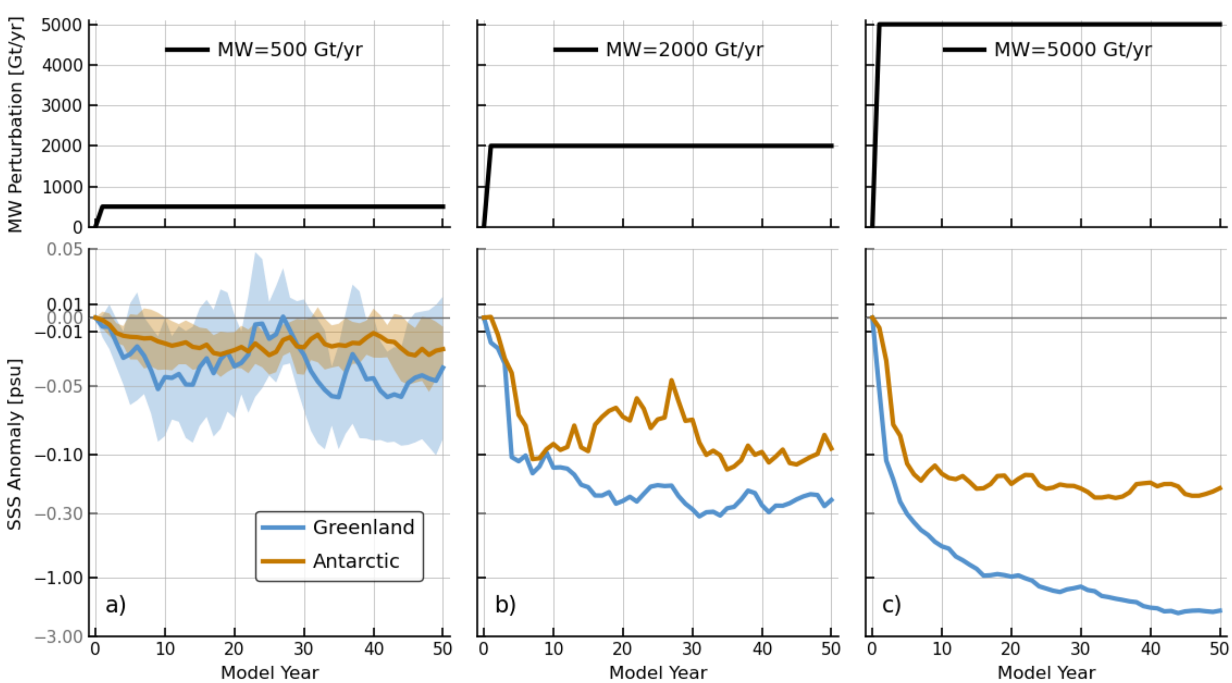

FIG. 1. Time series of step-change meltwater forcings of a) 500 Gt yr^{-1}, b) 2000 Gt yr^{-1} and c) 5000 Gt yr^{-1} and the resulting SSS anomalies (psu) around Greenland (45°–80°N, 5°–65°W) and Antarctica (50°–90°S, 0°–360°E) in the Greenland (blue) and Antarctic (orange) scenarios, respectively. In panel a), the shading represents one standard deviation model spread for 10 ensemble members and the line in the middle represents the ensemble mean in the 500 Gt yr^{-1} case. Note that in the bottom panels the y-axis SSS scale is non-linear.

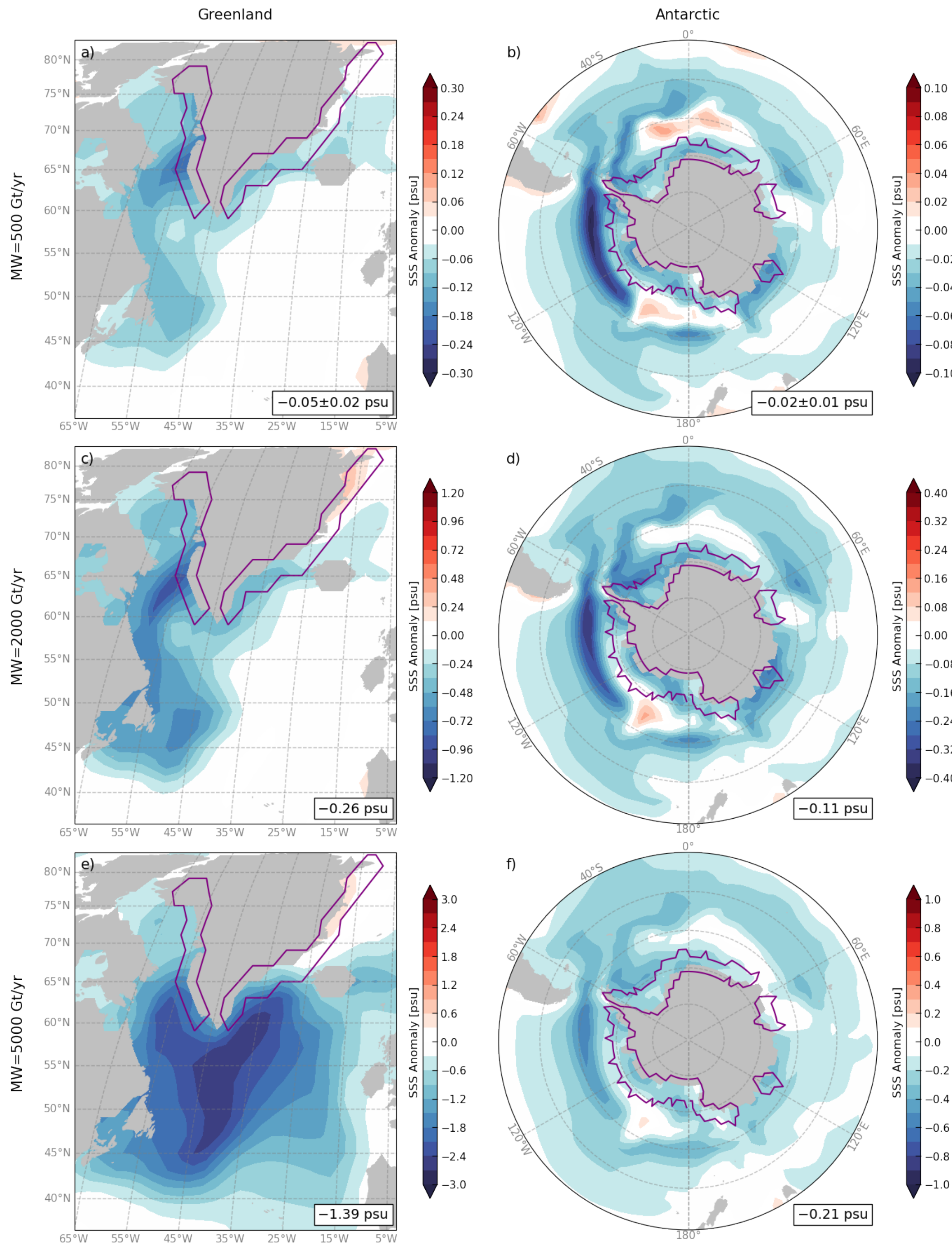

FIG. 2. SSS anomalies (psu) averaged over 50 years for a, c, e) the North Atlantic in the Greenland scenario and b, d, f) the Southern Ocean in the Antarctic scenario with meltwater forcings of 500 Gt yr^{-1}, 2000 Gt yr^{-1} and 5000 Gt yr^{-1}, respectively. Purple contours indicate the Greenland and Antarctic areas where glacial meltwater is fluxed into the ocean. Spatially-averaged SSS anomalies around Greenland (45°–80°N, 5°–65°W) and Antarctic (50°–90°S, 0°–360°E) areas (with one standard deviation for 10 ensemble members in the 500 Gt yr^{-1} case) are indicated in the tiny boxes.

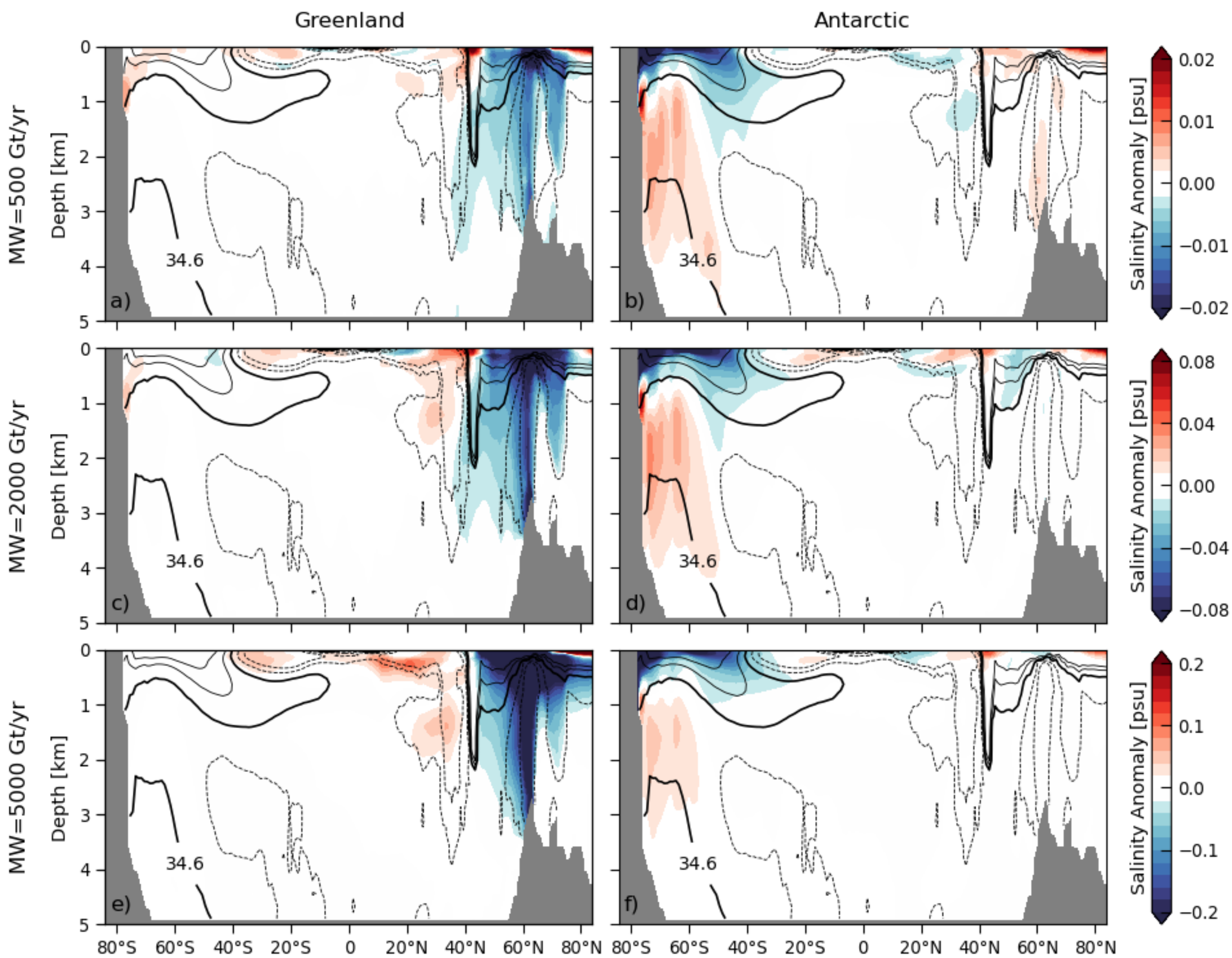

435 FIG. 3. Vertical cross-sections of zonal-mean ocean salinity anomalies (psu; color) averaged over 50 years in the a, c, e) Greenland and b, d, f) Antarctic scenarios with meltwater forcings of 500 Gt yr^{-1}, 2000 Gt yr^{-1} and 5000 Gt yr^{-1}, respectively. Contours represent the climatological-mean ocean salinity from the control runs with an interval of 0.2 psu. The bold line is the 34.6 psu contour, marking the low-salinity tongue of Antarctic Intermediate Water extending to depth in the mid-latitudes of the Southern Ocean. Dashed and solid contours denote values above and below 34.6 psu, respectively.

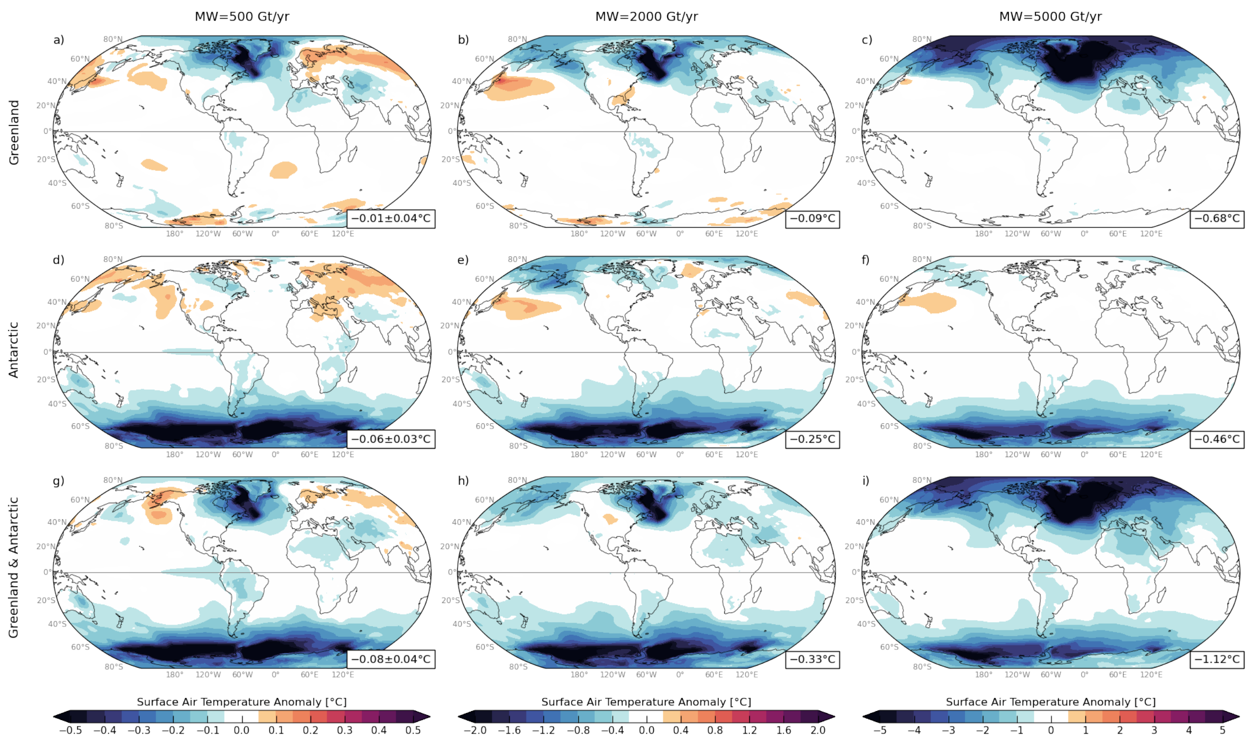

FIG. 4. Surface air temperature anomalies (°C) averaged over 50 years in the a, b, c) Greenland, d, e, f) Antarctic and g, h, i) simultaneous Greenland and Antarctic scenarios with meltwater forcings of 500 Gt yr^{-1}, 2000 Gt yr^{-1} and 5000 Gt yr^{-1}, respectively. Globally-averaged surface air temperature anomalies (with one standard deviation for 10 ensemble members in the 500 Gt yr^{-1} case) are indicated in the tiny boxes.

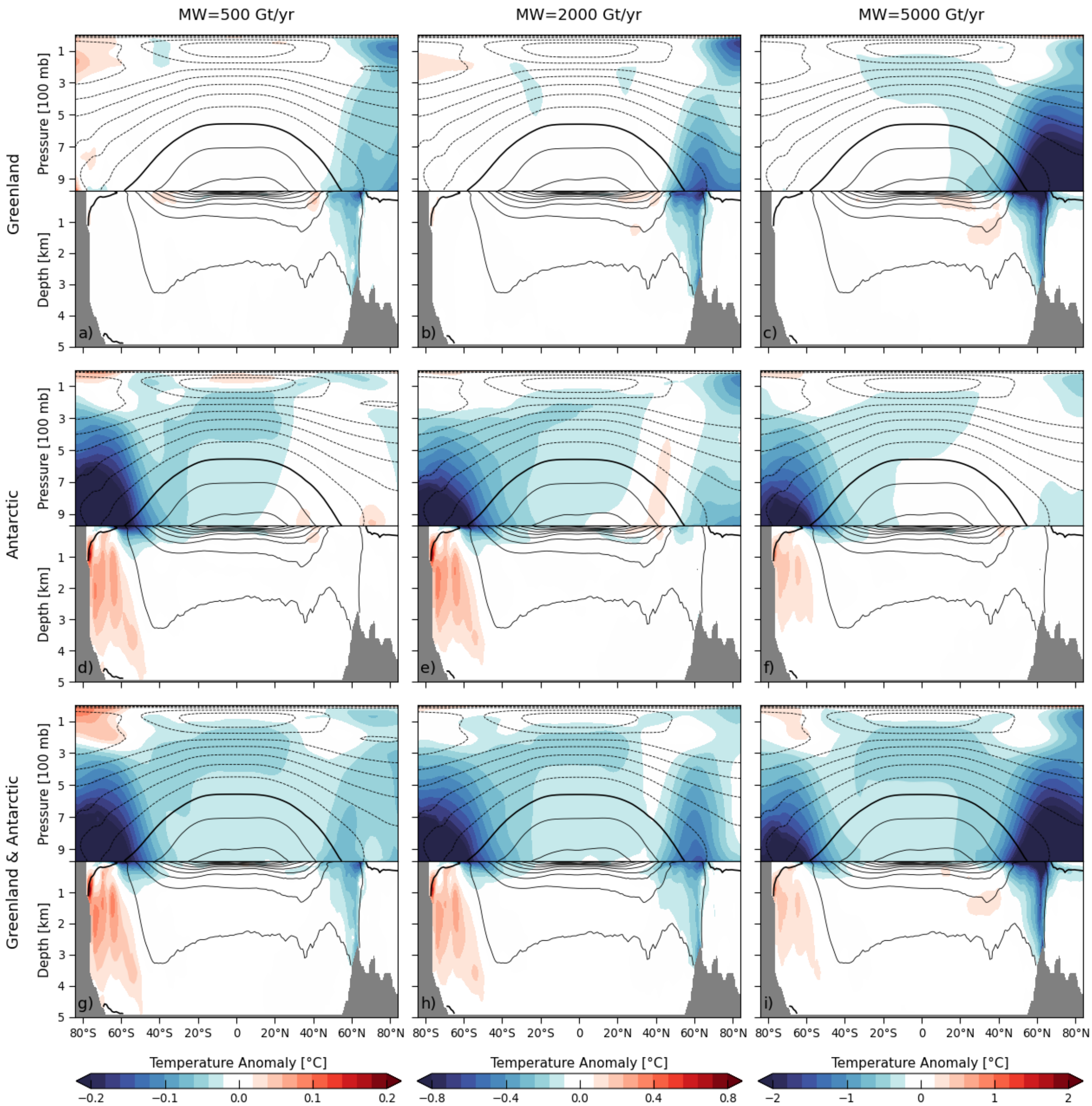

FIG. 5. Vertical cross-sections of zonal-mean atmospheric and ocean temperature anomalies (°C; color) averaged over 50 years in the a, b, c) Greenland, d, e, f) Antarctic and g, h, i) simultaneous Greenland and Antarctic scenarios with meltwater forcings of 500 Gt yr^{-1}, 2000 Gt yr^{-1} and 5000 Gt yr^{-1}, respectively. Contours represent the climatological-mean atmospheric and ocean temperature from the control runs with an interval of 10 °C and 3 °C, respectively. Dashed, solid and bold contours denote the negative, positive and zero values, respectively.

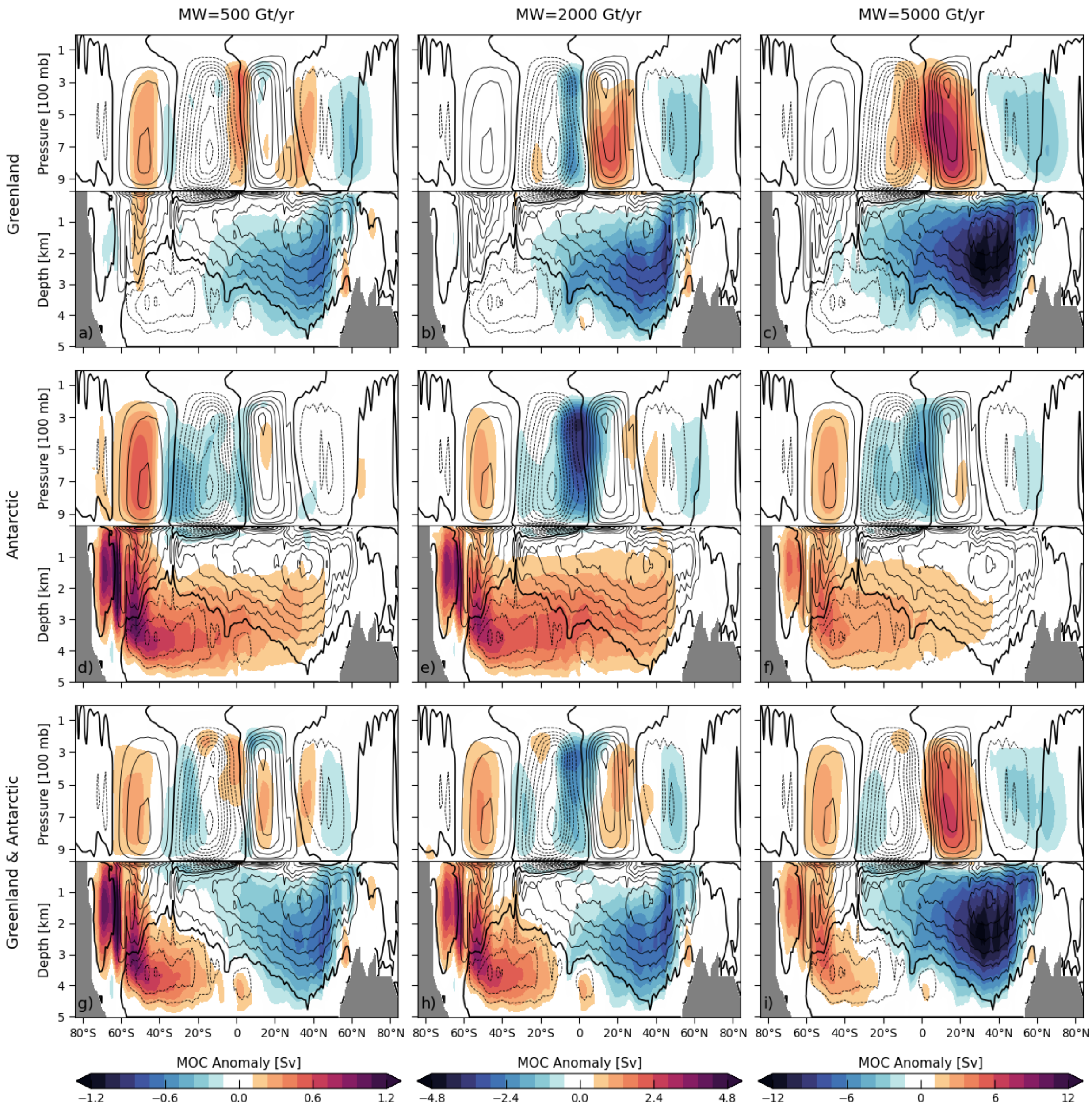

FIG. 6. Vertical cross-sections of zonal-mean atmospheric and ocean MOC anomalies (Sv; color) averaged over 50 years in the a, b, c) Greenland, d, e, f) Antarctic and g, h, i) simultaneous Greenland and Antarctic scenarios with the meltwater forcing of 500 Gt yr^{-1}, 2000 Gt yr^{-1} and 5000 Gt yr^{-1}, respectively. Contours represent the climatological mean atmospheric and ocean MOC from the control runs with an interval of 12 Sv and 4 Sv respectively. Dashed, solid and bold contours denote the negative (anticlockwise), positive (clockwise) and zero values, respectively.

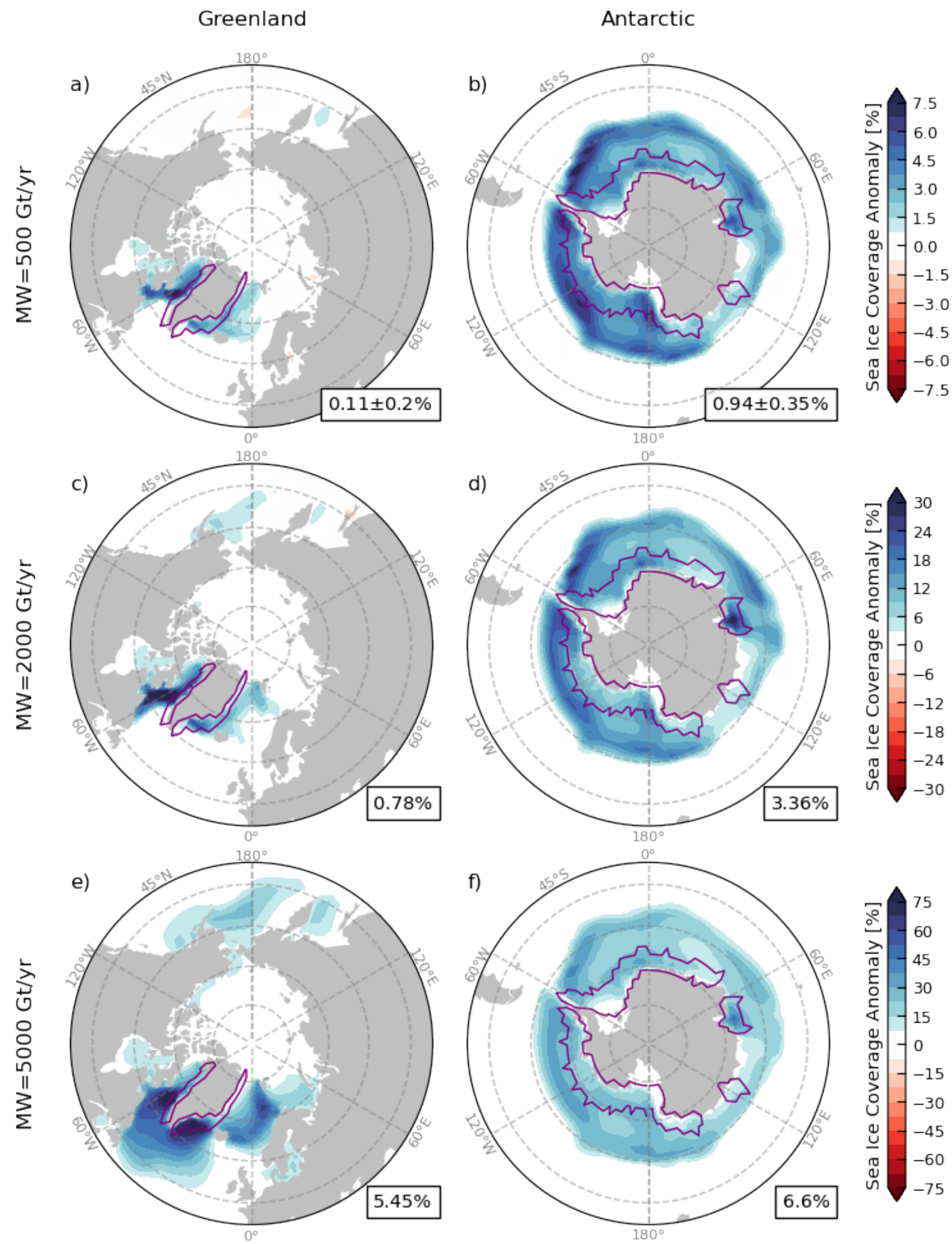

FIG. 7. Sea ice coverage anomalies (%) averaged over 50 years for a, c, e) the Northern Hemisphere (NH) in the Greenland scenario and b, d, f) the Southern Hemisphere (SH) in the Antarctic scenario with meltwater forcings of 500 Gt yr^{-1}, 2000 Gt yr^{-1} and 5000 Gt yr^{-1}, respectively. Purple contours indicate where glacial meltwater is fluxed into the ocean. Negative and positive values indicate the sea ice expansion and retreat, respectively. The NH (north of 45°N) and SH (south of 45°S) averages of sea ice coverage anomalies (with one standard deviation for 10 ensemble members in the 500 Gt yr^{-1} case) are indicated in the tiny boxes.

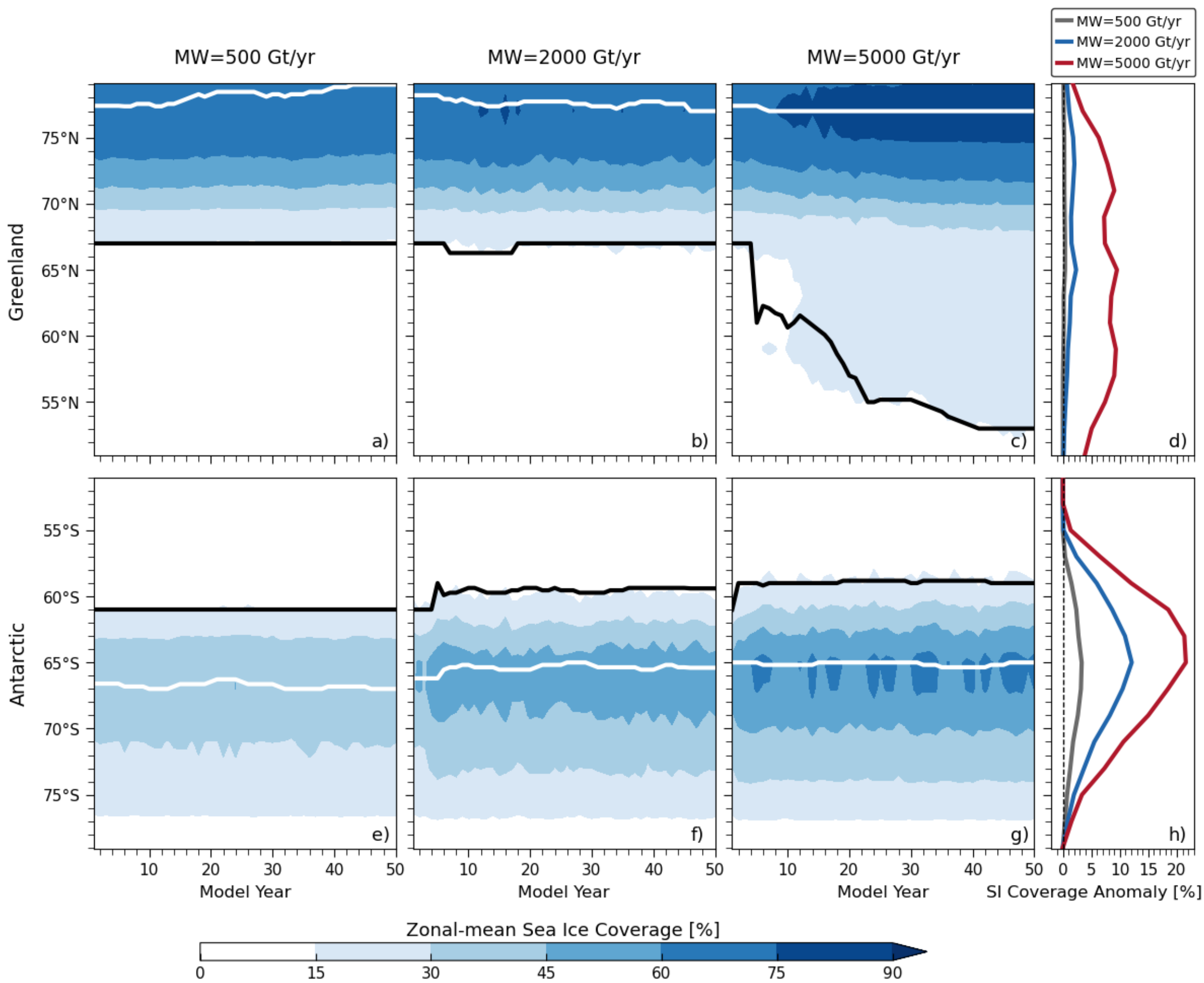

FIG. 8. Hovmöller diagram of zonal-mean sea ice coverage (%) over 50 years for a, b, c) the NH in the Greenland scenario and e, f, g) the SH in the Antarctic scenario with meltwater forcings of 500 Gt yr^{-1}, 2000 Gt yr^{-1} and 5000 Gt yr^{-1}, respectively. Zonal-mean sea ice coverage anomalies (%) averaged over 50 years for d) the NH in the Greenland scenario and h) the SH in the Antarctic scenario. Contours in a-c) and e-g) indicate the latitude of maximum (marked in white) and 15 percent (black) sea ice concentration after a 11-year moving average.

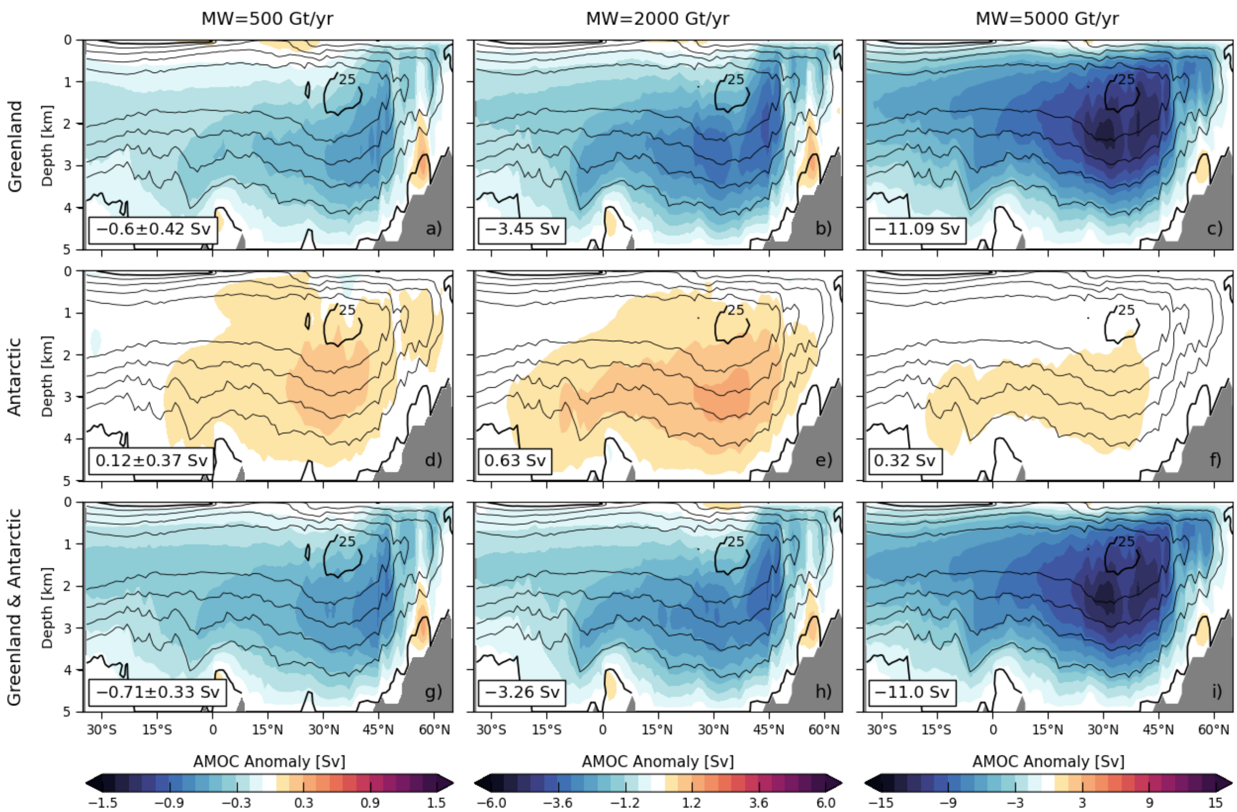

Fig. 9. Vertical cross-sections of zonal-mean AMOC anomalies (Sv; color) averaged over 50 years in the a, b, c) Greenland, d, e, f) Antarctic and g, h, i) simultaneous Greenland and Antarctic scenarios with the meltwater forcing of 500 Gt yr^{-1}, 2000 Gt yr^{-1} and 5000 Gt yr^{-1}, respectively. Contours represent the climatological mean AMOC with an interval of 5 Sv and values of 0 Sv and 5 Sv in bold from the control runs. AMOC strength anomalies (with one standard deviation for 10 ensemble members in the 500 Gt yr^{-1} case) are indicated in the tiny boxes.

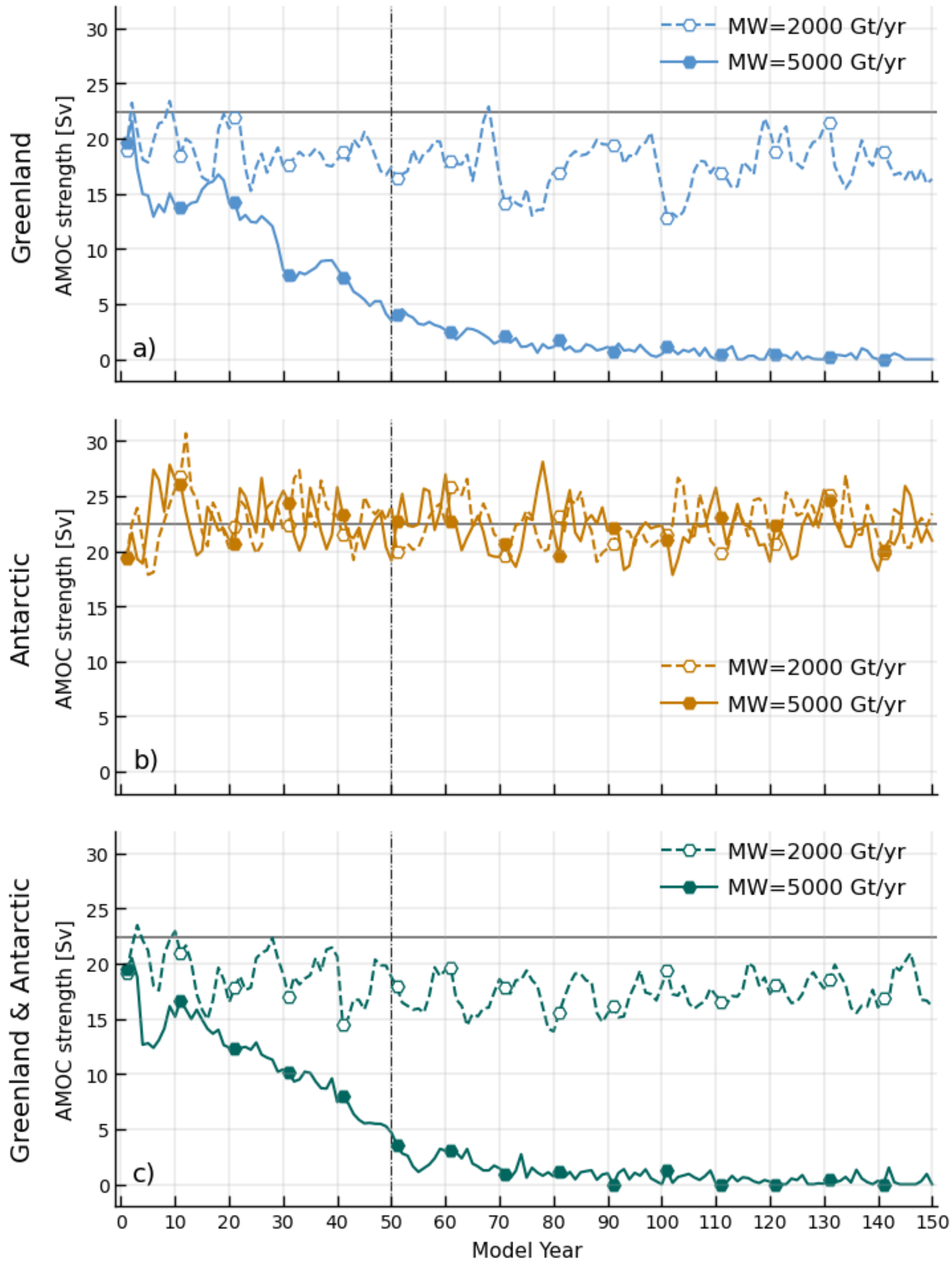

FIG. 10. Time series of AMOC strength (Sv) in the a) Greenland (blue line), b) Antarctic (orange line) and c) simultaneous Greenland and Antarctic (green line) scenarios with meltwater forcings of 2000 Gt yr^{-1} (dashed line with hollow circles) and 5000 Gt yr^{-1} (solid line with filled circles). Hollow and filled circles highlight the values every 10 years. The gray line denotes an AMOC strength of 22.45 Sv averaged over 150 years from the control run.

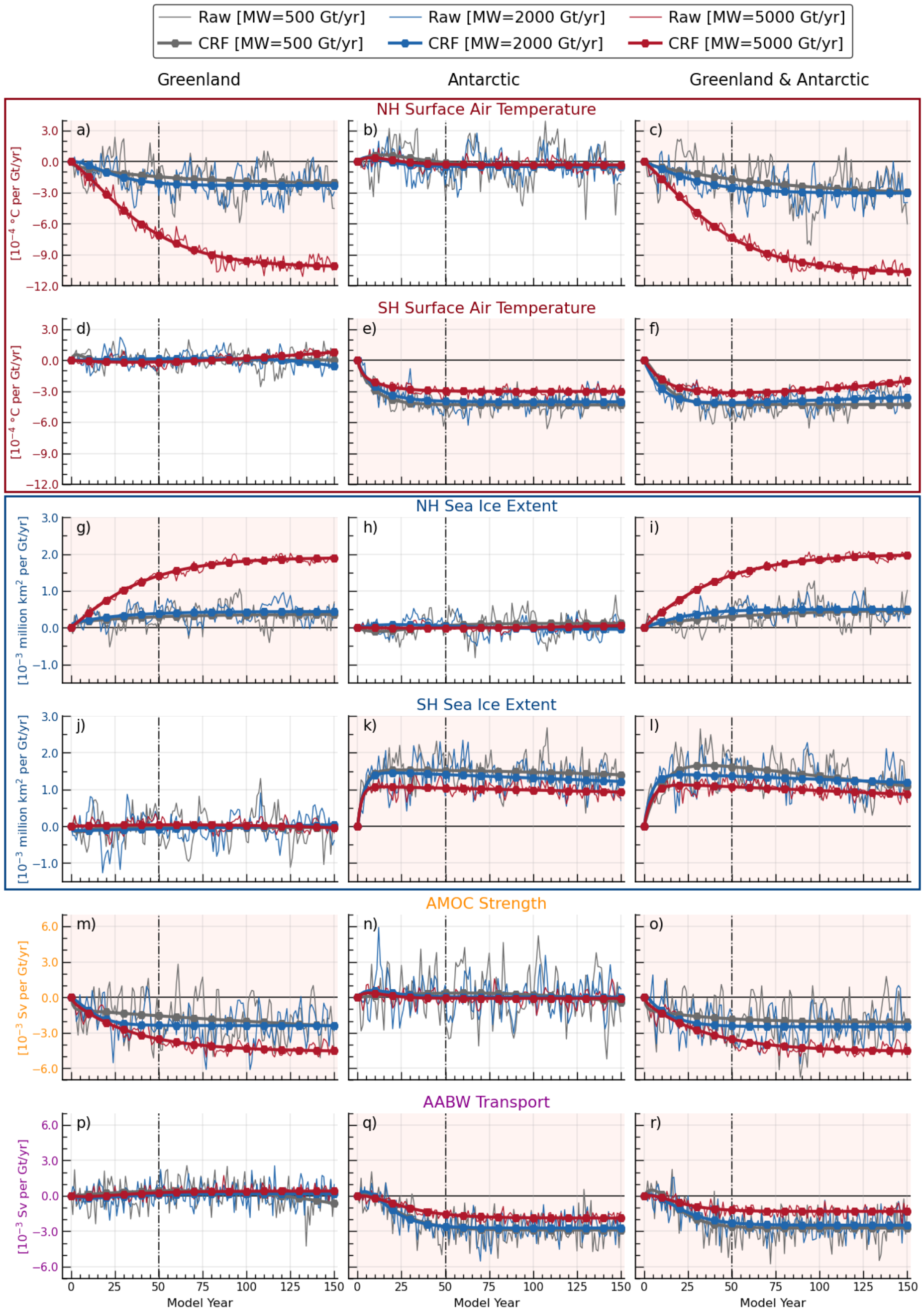

FIG. 11. Time series (dashed line) and fitted curves, representing the CRF (solid line) of the a, b, c) NH and d, e, f) SH surface air temperature (°C per Gt yr^{-1}), g, h, i) NH and j, k, l) SH sea ice extent (million km^2 per Gt yr^{-1}), m, n, o) AMOC strength (Sv per Gt yr^{-1}) and p, q, r) AABW transport anomalies (Sv per Gt yr^{-1}). Note that all curves are scaled per unit forcing for Greenland, Antarctic and simultaneous Greenland and Antarctic meltwater forcings of 500 Gt yr^{-1} (blue line), 2000 Gt yr^{-1} (gray line) and 5000 Gt yr^{-1} (red line), respectively. For the significant and persistent anomalies highlighted with light pink background shading, CRFs are estimated based on an exponential fit of raw time series. For the non-significant anomalies, the estimated CRFs based on an exponential fit are close to a zero-line. The NH and SH are defined as the region north of 23.5°N and south of 23.5°S, respectively, and thus exclude the tropics.

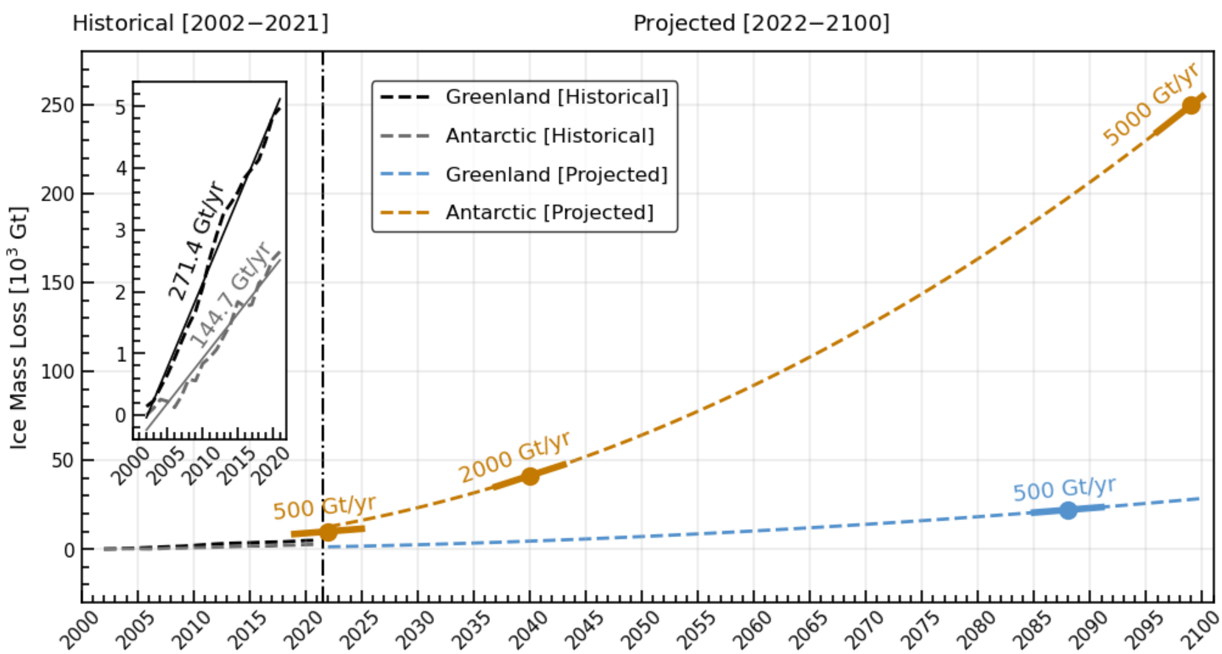

Fig. 12. Greenland and Antarctic ice mass loss anomalies (Gt; dashed line) relative to 2002 during the historical period 2002–2021 (Watkins et al. 2015) and projected forward from 2022–2100 under the RCP8.5 scenario (Golledge et al. 2019). The inside box is a zoom on the historical period: black and gray solid lines represent a linear regression of historical anomalies yielding a constant ice mass loss rate of 271.4 Gt yr^{-1} and 144.7 Gt yr^{-1} for Greenland and Antarctica, respectively. During the remainder of the century, the projected mass loss over Greenland reaches 500 Gt yr^{-1} around 2088, and the mass loss over Antarctic is projected to be 500 Gt yr^{-1}, 2000 Gt yr^{-1} and 5000 Gt yr^{-1} in 2022, 2040 and 2099, respectively.

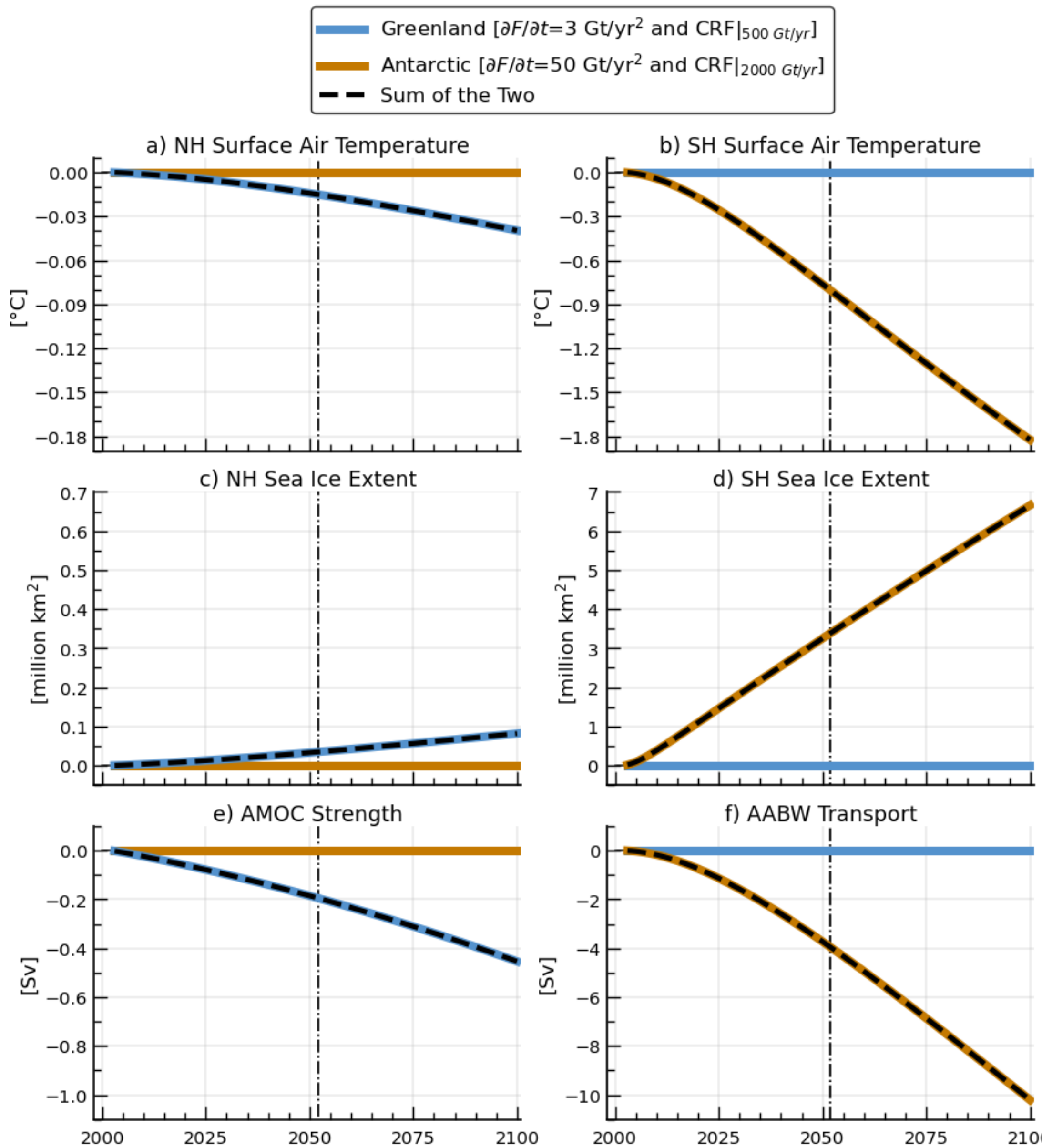

FIG. 13. Projections based on linear convolution for the a) NH and b) SH surface air temperature anomalies (°C), c) NH and d) SH sea ice extent anomalies (million km^2), e) AMOC strength anomalies (Sv) and f) AABW transport anomalies (Sv). The blue solid line is the projection in response to Greenland melt, assuming a $\partial F/\partial t$ of 3 Gt yr^{-2} using a CRF from the 500 Gt yr^{-1}. The orange solid line is the projection in response to Antarctic melt, assuming $\partial F/\partial t$ = 50 Gt yr^{-2} and the CRF from the 2000 Gt yr^{-1}. The black dashed line is the sum of the two.

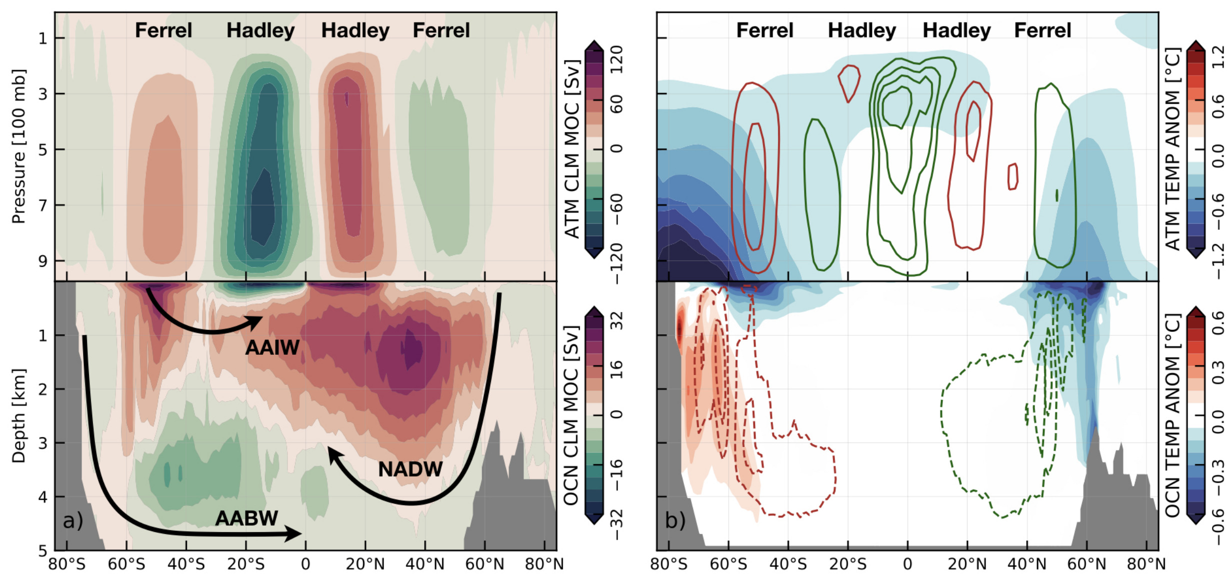

FIG. 14. Summary figure showing the response of the climate to glacial melt based on 50-year averages from simulations in which glacial melt over both Greenland and Antarctic was applied as a step-function with a magnitude of 2000 Gt yr^{-1}. The lhs (labeled a) shows the climatological state of the atmosphere (top) and ocean (bottom): the rhs (labeled b) shows changes in key quantities. Key circulation patterns are also labeled and indicated by arrows. Green contours indicate anticlockwise circulation; red contours clockwise circulation. Continuous contours indicate a strengthening of the preexisting circulation; dashed contours a weakening. Quantities plotted are vertical cross-sections of zonal-mean a) climatological mean atmospheric MOC (Sv; color and black contours; top panel) and ocean MOC (Sv; color; bottom panel) from the control run, and b) atmospheric MOC (Sv; color-coded contours) and temperature (°C; color) anomalies (top panel) and ocean MOC (Sv; color-coded contours) and temperature (°C; color) anomalies (bottom panel). Darkgreen and deepred solid contours in the top panel of b) respectively show the negative and positive values of atmospheric MOC anomalies from -2.4 Sv to 1.2 Sv with an interval of 0.6 Sv: these represent *enhanced* Hadley and Ferrel cells. Darkgreen and deepred dashed contours in the bottom panel of b) show the negative and positive values of ocean MOC anomalies from -3 Sv to 3 Sv with an interval of 1.5 Sv: these represent *weakened* upper and lower cells.

Acknowledgments. QL, JM, CR and AR are supported by the NASA MAP program 19-MAP19-0011 and the MIT-GISS cooperative agreement. The model simulations and analysis were conducted on the NASA High-End Computing (HEC) Program through the NASA Center for Climate Simulation (NCCS) at Goddard Space Flight Center.

Data availability statement. The data sets analyzed in this study will be all publicly available. Model components are all open source. The GISS modelE is available at `https://www.giss.nasa.gov/tools/modelE/`. The Greenland and Antarctic ice mass data from satellite observations were obtained for the period 2002–2021 at `https://climate.nasa.gov/vital-signs/ice-sheets/`.

References

Adusumilli, S., H. A. Fricker, B. Medley, L. Padman, and M. R. Siegfried, 2020: Interannual variations in meltwater input to the Southern Ocean from Antarctic ice shelves. *Nature Geoscience*, **13 (9)**, 616–620, https://doi.org/10.1038/s41561-020-0616-z.

Bakker, P., and M. Prange, 2018: Response of the intertropical convergence zone to Antarctic ice sheet melt. *Geophysical Research Letters*, **45 (16)**, 8673–8680, https://doi.org/https://doi.org/10.1029/2018GL078659.

Bellomo, K., M. Angeloni, S. Corti, and J. von Hardenberg, 2021: Future climate change shaped by inter-model differences in Atlantic meridional overturning circulation response. *Nature communications*, **12 (1)**, 3659–3659, https://doi.org/10.1038/s41467-021-24015-w.

Bintanja, R., G. J. van Oldenborgh, S. S. Drijfhout, B. Wouters, and C. A. Katsman, 2013: Important role for ocean warming and increased ice-shelf melt in Antarctic sea-ice expansion. *Nature Geoscience*, **6 (5)**, 376–379, https://doi.org/10.1038/ngeo1767.

Bitz, C. M., and W. H. Lipscomb, 1999: An energy-conserving thermodynamic model of sea ice. *Journal of Geophysical Research: Oceans*, **104 (C7)**, 15 669–15 677, https://doi.org/https://doi.org/10.1029/1999JC900100.

Boers, N., 2021: Observation-based early-warning signals for a collapse of the atlantic meridional overturning circulation. *Nature Climate Change*, **11 (8)**, 680–688, https://doi.org/10.1038/s41558-021-01097-4.

Böning, C. W., E. Behrens, A. Biastoch, K. J. Getzlaff, and J. L. Bamber, 2016: Emerging impact of Greenland meltwater on deepwater formation in the North Atlantic Ocean. *Nature Geoscience*, **9 (7)**, 523–527, https://doi.org/10.1038/ngeo2740.

Bronselaer, B., M. Winton, S. M. Griffies, W. J. Hurlin, K. B. Rodgers, O. V. Sergienko, R. J. Stouffer, and J. L. Russell, 2018: Change in future climate due to Antarctic meltwater. *Nature*, **564 (7734)**, 53–58, https://doi.org/10.1038/s41586-018-0712-z.

Buckley, M. W., and J. Marshall, 2016: Observations, inferences, and mechanisms of the Atlantic Meridional Overturning Circulation: A review. *Reviews of Geophysics*, **54 (1)**, 5–63, https://doi.org/https://doi.org/10.1002/2015RG000493.

Caesar, L., S. Rahmstorf, A. Robinson, G. Feulner, and V. Saba, 2018: Observed fingerprint of a weakening Atlantic Ocean overturning circulation. *Nature*, **556 (7700)**, 191–196, https://doi.org/10.1038/s41586-018-0006-5.

Czaja, A., and J. Marshall, 2006: The partitioning of poleward heat transport between the atmosphere and ocean. *Journal of the Atmospheric Sciences*, **63 (5)**, 1498–1511, https://doi.org/10.1175/JAS3695.1.

DeConto, R. M., and D. Pollard, 2016: Contribution of Antarctica to past and future sea-level rise. *Nature*, **531 (7596)**, 591–597, https://doi.org/10.1038/nature17145.

Delworth, T., S. Manabe, and R. J. Stouffer, 1993: Interdecadal variations of the thermohaline circulation in a coupled ocean-atmosphere model. *Journal of Climate*, **6 (11)**, 1993–2011, https://doi.org/10.1175/1520-0442(1993)006<1993:IVOTTC>2.0.CO;2.

Depoorter, M. A., J. L. Bamber, J. A. Griggs, J. T. M. Lenaerts, S. R. M. Ligtenberg, M. R. van den Broeke, and G. Moholdt, 2013: Calving fluxes and basal melt rates of Antarctic ice shelves. *Nature*, **502 (7469)**, 89–92, https://doi.org/10.1038/nature12567.

Eyring, V., S. Bony, G. A. Meehl, C. A. Senior, B. Stevens, R. J. Stouffer, and K. E. Taylor, 2016: Overview of the Coupled Model Intercomparison Project Phase 6 (CMIP6) experimental design and organization. *Geoscientific Model Development*, **9 (5)**, 1937–1958, https://doi.org/10.5194/gmd-9-1937-2016.

Fretwell, P., and Coauthors, 2013: Bedmap2: improved ice bed, surface and thickness datasets for Antarctica. *The Cryosphere*, **7 (1)**, 375–393, https://doi.org/10.5194/tc-7-375-2013.

Gent, P. R., J. Willebrand, T. J. McDougall, and J. C. McWilliams, 1995: Parameterizing eddy-induced tracer transports in ocean circulation models. *Journal of Physical Oceanography*, **25 (4)**, 463–474, https://doi.org/10.1175/1520-0485(1995)025<0463:PEITTI>2.0.CO;2.

Golledge, N. R., E. D. Keller, N. Gomez, K. A. Naughten, J. Bernales, L. D. Trusel, and T. L. Edwards, 2019: Global environmental consequences of twenty-first-century ice-sheet melt. *Nature*, **566 (7742)**, 65–72, https://doi.org/10.1038/s41586-019-0889-9.

Hasselmann, K., R. Sausen, E. Maier-Reimer, and R. Voss, 1993: On the cold start problem in transient simulations with coupled atmosphere-ocean models. *Climate Dynamics*, **9 (2)**, 53–61, https://doi.org/10.1007/BF00210008.

Hellmer, H. H., 2004: Impact of Antarctic ice shelf basal melting on sea ice and deep ocean properties. *Geophysical Research Letters*, **31 (10)**, https://doi.org/https://doi.org/10.1029/2004GL019506.

Hu, A., G. A. Meehl, W. Han, and J. Yin, 2011: Effect of the potential melting of the Greenland ice sheet on the meridional overturning circulation and global climate in the future. *Deep Sea Research Part II: Topical Studies in Oceanography*, **58 (17)**, 1914–1926, https://doi.org/https://doi.org/10.1016/j.dsr2.2010.10.069.

Kelley, M., and Coauthors, 2020: GISS-E2.1: Configurations and climatology. *Journal of Advances in Modeling Earth Systems*, **12 (8)**, e2019MS002 025, https://doi.org/https://doi.org/10.1029/2019MS002025.

Lago, V., and M. H. England, 2019: Projected slowdown of Antarctic Bottom Water formation in response to amplified meltwater contributions. *Journal of Climate*, **32 (19)**, 6319–6335, https://doi.org/10.1175/JCLI-D-18-0622.1.

Large, W. G., J. C. McWilliams, and S. C. Doney, 1994: Oceanic vertical mixing: A review and a model with a nonlocal boundary layer parameterization. *Reviews of Geophysics*, **32 (4)**, 363–403, https://doi.org/https://doi.org/10.1029/94RG01872.

Lerner, P., A. Romanou, M. Kelley, J. Romanski, R. Ruedy, and G. Russell, 2021: Drivers of air-sea CO_2 flux seasonality and its long-term changes in the NASA-GISS model CMIP6 submission. *Journal of Advances in Modeling Earth Systems*, **13 (2)**, e2019MS002 028, https://doi.org/https://doi.org/10.1029/2019MS002028.

Li, Q., M. H. England, A. M. Hogg, S. R. Rintoul, and A. K. Morrison, 2022: Future abyssal ocean warming driven by glacial melt. *Submitted*.

Lozier, M. S., and Coauthors, 2019: A sea change in our view of overturning in the subpolar North Atlantic. *Science*, **363 (6426)**, 516–521, https://doi.org/10.1126/science.aau6592.

Mackie, S., I. J. Smith, J. K. Ridley, D. P. Stevens, and P. J. Langhorne, 2020: Climate response to increasing Antarctic iceberg and ice shelf melt. *Journal of Climate*, **33 (20)**, 8917–8938, https://doi.org/10.1175/JCLI-D-19-0881.1.

Marshall, J., K. C. Armour, J. R. Scott, Y. Kostov, U. Hausmann, D. Ferreira, T. G. Shepherd, and C. M. Bitz, 2014: The ocean's role in polar climate change: asymmetric Arctic and Antarctic responses to greenhouse gas and ozone forcing. *Philosophical Transactions of the Royal Society A: Mathematical, Physical and Engineering Sciences*, **372 (2019)**, 20130 040, https://doi.org/10.1098/rsta.2013.0040.

Marshall, J., J. Scott, and A. Proshutinsky, 2017a: "Climate response functions" for the Arctic ocean: a proposed coordinated modelling experiment. *Geoscientific Model Development*, **10 (7)**, 2833–2848, https://doi.org/10.5194/gmd-10-2833-2017.

Marshall, J., J. R. Scott, A. Romanou, M. Kelley, and A. Leboissetier, 2017b: The dependence of the ocean's MOC on mesoscale eddy diffusivities: A model study. *Ocean Modelling*, **111**, 1–8, https://doi.org/https://doi.org/10.1016/j.ocemod.2017.01.001.

Marshall, J., and K. Speer, 2012: Closure of the meridional overturning circulation through Southern Ocean upwelling. *Nature Geoscience*, **5 (3)**, 171–180, https://doi.org/10.1038/ngeo1391.

Marson, J. M., L. C. Gillard, and P. G. Myers, 2021: Distinct ocean responses to Greenland's liquid runoff and iceberg melt. *Journal of Geophysical Research: Oceans*, **126 (12)**, e2021JC017 542, https://doi.org/https://doi.org/10.1029/2021JC017542.

Miller, R. L., and Coauthors, 2021: Cmip6 historical simulations (1850–2014) with GISS-E2.1. *Journal of Advances in Modeling Earth Systems*, **13 (1)**, e2019MS002 034, https://doi.org/https://doi.org/10.1029/2019MS002034.

Moorman, R., A. K. Morrison, and A. M. Hogg, 2020: Thermal responses to Antarctic ice shelf melt in an eddy-rich global ocean–sea ice model. *Journal of Climate*, **33 (15)**, 6599–6620, https://doi.org/10.1175/JCLI-D-19-0846.1.

Morlighem, M., and Coauthors, 2017: Bedmachine v3: Complete bed topography and ocean bathymetry mapping of Greenland from multibeam echo sounding combined with mass conservation. *Geophysical Research Letters*, **44 (21)**, 11,051–11,061, https://doi.org/https://doi.org/10.1002/2017GL074954.

Mouginot, J., and Coauthors, 2019: Forty-six years of Greenland ice sheet mass balance from 1972 to 2018. *Proceedings of the National Academy of Sciences*, **116 (19)**, 9239–9244, https://doi.org/10.1073/pnas.1904242116.

Nazarenko, L. S., and Coauthors, 2022: Future climate change under ssp emission scenarios with giss-e2.1. *Journal of Advances in Modeling Earth Systems*, **In press**, e2021MS002 871, https://doi.org/https://doi.org/10.1029/2021MS002871.

Orihuela-Pinto, B., M. H. England, and A. S. Taschetto, 2022: Interbasin and interhemispheric impacts of a collapsed Atlantic Overturning Circulation. *Nature Climate Change*, **In press**, https://doi.org/10.1038/s41558-022-01380-y.

Paolo, F. S., H. A. Fricker, and L. Padman, 2015: Volume loss from Antarctic ice shelves is accelerating. *Science*, **348 (6232)**, 327–331, https://doi.org/10.1126/science.aaa0940.

Pauling, A. G., C. M. Bitz, I. J. Smith, and P. J. Langhorne, 2016: The response of the Southern Ocean and Antarctic sea ice to freshwater from ice shelves in an earth system model. *Journal of Climate*, **29 (5)**, 1655–1672, https://doi.org/10.1175/JCLI-D-15-0501.1.

Pickart, R. S., and M. A. Spall, 2007: Impact of Labrador Sea convection on the North Atlantic meridional overturning circulation. *Journal of Physical Oceanography*, **37 (9)**, 2207–2227, https://doi.org/10.1175/JPO3178.1.

Prather, M. J., 1986: Numerical advection by conservation of second-order moments. *Journal of Geophysical Research: Atmospheres*, **91 (D6)**, 6671–6681, https://doi.org/https://doi.org/10.1029/JD091iD06p06671.

Purkey, S. G., and G. C. Johnson, 2010: Warming of global abyssal and deep Southern Ocean waters between the 1990s and 2000s: Contributions to global heat and sea level rise budgets. *Journal of Climate*, **23 (23)**, 6336–6351, https://doi.org/10.1175/2010JCLI3682.1.

Putrasahan, D. A., K. Lohmann, J.-S. von Storch, J. H. Jungclaus, O. Gutjahr, and H. Haak, 2019: Surface flux drivers for the slowdown of the Atlantic Meridional Overturning Circulation in a high-resolution global coupled climate model. *Journal of Advances in Modeling Earth Systems*, **11 (5)**, 1349–1363, https://doi.org/https://doi.org/10.1029/2018MS001447.

Rahmstorf, S., J. E. Box, G. Feulner, M. E. Mann, A. Robinson, S. Rutherford, and E. J. Schaffernicht, 2015: Exceptional twentieth-century slowdown in Atlantic Ocean overturning circulation. *Nature Climate Change*, **5 (5)**, 475–480, https://doi.org/10.1038/nclimate2554.

Rignot, E., S. Jacobs, J. Mouginot, and B. Scheuchl, 2013: Ice-shelf melting around Antarctica. *Science*, **341 (6143)**, 266–270, https://doi.org/10.1126/science.1235798.

Rignot, E., J. Mouginot, B. Scheuchl, M. van den Broeke, M. J. van Wessem, and M. Morlighem, 2019: Four decades of Antarctic ice sheet mass balance from 1979–2017. *Proceedings of the National Academy of Sciences*, **116 (4)**, 1095–1103, https://doi.org/10.1073/pnas.1812883116.

Russell, G. L., J. R. Miller, and D. Rind, 1995: A coupled atmosphere-ocean model for transient climate change studies. *Atmosphere-Ocean*, **33 (4)**, 683–730, https://doi.org/10.1080/07055900.1995.9649550.

Rye, C. D., J. Marshall, M. Kelley, G. Russell, L. S. Nazarenko, Y. Kostov, G. A. Schmidt, and J. Hansen, 2020: Antarctic glacial melt as a driver of recent Southern Ocean climate trends. *Geophysical Research Letters*, **47 (11)**, e2019GL086 892, https://doi.org/https://doi.org/10.1029/2019GL086892.

Rye, C. D., J. Marshall, D. Rind, G. A. Schmidt, and J. E. Hansen, 2022: Partial mitigation of global warming through Antarctic meltwater anomalies. *Science Advances*, **In revision**.

Schmidt, G. A., and Coauthors, 2014: Configuration and assessment of the giss modele2 contributions to the cmip5 archive. *Journal of Advances in Modeling Earth Systems*, **6 (1)**, 141–184, https://doi.org/https://doi.org/10.1002/2013MS000265.

Shepherd, A., and Coauthors, 2018: Mass balance of the Antarctic ice sheet from 1992 to 2017. *Nature*, **558 (7709)**, 219–222, https://doi.org/10.1038/s41586-018-0179-y.

Shepherd, A., and Coauthors, 2020: Mass balance of the Greenland ice sheet from 1992 to 2018. *Nature*, **579 (7798)**, 233–239, https://doi.org/10.1038/s41586-019-1855-2.

Silvano, A., S. R. Rintoul, B. Peña-Molino, W. R. Hobbs, E. van Wijk, S. Aoki, T. Tamura, and G. D. Williams, 2018: Freshening by glacial meltwater enhances melting of ice shelves and reduces formation of Antarctic Bottom Water. *Science Advances*, **4 (4)**, eaap9467, https://doi.org/10.1126/sciadv.aap9467.

Slater, T., A. E. Hogg, and R. Mottram, 2020: Ice-sheet losses track high-end sea-level rise projections. *Nature Climate Change*, **10 (10)**, 879–881, https://doi.org/10.1038/s41558-020-0893-y.

Stouffer, R. J., D. Seidov, and B. J. Haupt, 2007: Climate response to external sources of freshwater: North Atlantic versus the Southern Ocean. *Journal of Climate*, **20 (3)**, 436–448, https://doi.org/10.1175/JCLI4015.1.

Swingedouw, D., M.-N. Houssais, C. Herbaut, A.-C. Blaizot, M. Devilliers, and J. Deshayes, 2022: AMOC recent and future trends: A crucial role for oceanic resolution and Greenland melting? *Frontiers in Climate*, **4**, https://doi.org/10.3389/fclim.2022.838310.

Thompson, A. F., A. L. Stewart, P. Spence, and K. J. Heywood, 2018: The Antarctic Slope Current in a changing climate. *Reviews of Geophysics*, **56 (4)**, 741–770, https://doi.org/https://doi.org/10.1029/2018RG000624.

Thornalley, D. J. R., and Coauthors, 2018: Anomalously weak Labrador Sea convection and Atlantic overturning during the past 150 years. *Nature*, **556 (7700)**, 227–230, https://doi.org/10.1038/s41586-018-0007-4.

Tournadre, J., N. Bouhier, F. Girard-Ardhuin, and F. Rémy, 2016: Antarctic icebergs distributions 1992–2014. *Journal of Geophysical Research: Oceans*, **121 (1)**, 327–349, https://doi.org/https://doi.org/10.1002/2015JC011178.

Visbeck, M., J. Marshall, T. Haine, and M. Spall, 1997: Specification of eddy transfer coefficients in coarse-resolution ocean circulation models. *Journal of Physical Oceanography*, **27 (3)**, 381–402, https://doi.org/10.1175/1520-0485(1997)027<0381:SOETCI>2.0.CO;2.

Watkins, M. M., D. N. Wiese, D.-N. Yuan, C. Boening, and F. W. Landerer, 2015: Improved methods for observing Earth's time variable mass distribution with GRACE using spherical cap mascons. *Journal of Geophysical Research: Solid Earth*, **120 (4)**, 2648–2671, https://doi.org/https://doi.org/10.1002/2014JB011547.

Weaver, A. J., O. A. Saenko, P. U. Clark, and J. X. Mitrovica, 2003: Meltwater pulse 1A from Antarctica as a trigger of the Bølling-Allerød warm interval. *Science*, **299 (5613)**, 1709–1713, https://doi.org/10.1126/science.1081002.

Weijer, W., M. E. Maltrud, M. W. Hecht, H. A. Dijkstra, and M. A. Kliphuis, 2012: Response of the Atlantic Ocean circulation to Greenland ice sheet melting in a strongly-eddying ocean model. *Geophysical Research Letters*, **39 (9)**, https://doi.org/https://doi.org/10.1029/2012GL051611.

Zhang, J., 2007: Increasing Antarctic sea ice under warming atmospheric and oceanic conditions. *Journal of Climate*, **20 (11)**, 2515–2529, https://doi.org/10.1175/JCLI4136.1.

Zhang, J., and D. Rothrock, 2000: Modeling Arctic sea ice with an efficient plastic solution. *Journal of Geophysical Research: Oceans*, **105 (C2)**, 3325–3338, https://doi.org/https://doi.org/10.1029/1999JC900320.